Desalination and Water Treatment
www.deswater.com

doi: 10.5004/dwt.2023.29455

290 (2023) 128–146
April

Grapevine wood biomass as a new bio-adsorbent for methylene blue: equilibrium, thermodynamic, kinetic, and isotherm analyses, both linear and non-linear

Rachida Souidi[a], Yasmina Khane[a,b,*], Khedidja Benouis[c], Lahcene Belarbi[a], Salim Albukhaty[d], Mustafa K.A. Mohammed[e], Smain Bousalem[a]

[a]*Applied Chemistry Laboratory, University of Ain Temouchent, Bp 284, Ain Temouchent 46000, Algeria, emails: souidirachida@yahoo.fr (R. Souidi), lahcen.belarbi@univ-temouchent.edu.dz (L. Belarbi), smainchem@gmail.com (S. Bousalem)*
[b]*Universite de Ghardaia, BP 455, Ghardaïa, 47000, Algeria, emails: yasminekhane@yahoo.fr/ yasmine@univ-ghardaia.dz/yasminekhane@yahoo.com (Y. Khane)*
[c]*Laboratory of Process Engineering, Materials, and Environment, Department of Energy and Process Engineering, Faculty of Technology, University of Djillali Liabes, Sidi Bel Abbes, P.O. Box: 89 SBA 22000, Algeria, email: benouis_khadidja@yahoo.fr (K. Benouis)*
[d]*Department of Chemistry, College of Science, University of Misan, Maysan 62001, Iraq, email: albukhaty.salim@uomisan.edu.iq (S. Albukhaty)*
[e]*College of Remote Sensing and Geophysics, Al-Karkh University of Science, Al-Karkh Side, Haifa St. Hamada Palace, Beghdad 10011, Iraq, email: mustafa.kareem@uomus.edu.iq (M.K.A. Mohammed)*

Received 25 November 2022; Accepted 7 March 2023

ABSTRACT

Recent studies have focused a significant amount of attention on the problem of dyes in water because of their adverse outcomes for the environment and people's life. In the current work, the adsorption capacity of the sawdust of grapevine wood (GVW) from agricultural waste was employed as a new inexpensive, and green biosorbent via a batch adsorption process. Sulfuric acid was applied to grapevine wood to activate the sorbents for methylene blue (MB) elimination from the solution medium under varied parameters, including temperature, pH, original MB content, contact time, and adsorbent dimensions. The optimum capacity for adsorption (q_{max}) of 220.51 mg·g^{-1} at 293 K was obtained after 180 min of solid/liquid contact with 1 g·L^{-1} activated grapevine wood (GVWA) sawdust. The Freundlich and pseudo-second-order systems were given the optimal isotherm and kinetic results for MB biosorption onto GVWA sawdust using linear and non-linear regression techniques. The findings for MB biosorption exhibit that non-linear regression was the best approach to choosing the optimum kinetic and isotherm models. The calculated standards for entropy change, standard enthalpy change, and standard Gibbs free energy change demonstrated that the adsorption dynamic was exothermic, spontaneous, and advantageous. Our findings suggest that sustainable and cost-effective GVWA is a suitable candidate for removing emerging contaminants like MB from contaminated waters.

Keywords: Grapevine wood; Chemical activation; Methylene blue; Adsorption; Linear and non-linear regression

* Corresponding author.

1. Introduction

Textile, cosmetics, plastics, rubber, printing, food, pharmaceutical, and dyeing industries are just a few of the many industries that use dyes [1,2]. Over 100 hundred dyes and 7 × 10^5 tons are produced worldwide. During production and processing, 10%–15% of artificial colors are lost, and 12% are thrown. Biodegradation is impossible because the textile industry's effluent is steady and complicated. The small amount of dye (<1 ppm) in water can block sunlight and disrupt undersea metabolism [3,4]. The dye is one of the most significant pollutant groups after their discharge into the open atmosphere without any appropriate treatment, because its complex chemical structure makes them very persistent and difficult to biodegrade [5]. These dyes are toxic to humans, animals, fish, and other aquatic organisms, as well as to the environment [6].

Recently, various methods, such as photodegradation, membrane filtration, precipitation, Fenton-biological, and coagulation–flocculation treatment, have been used to remove dyes from waste streams [7–9]. However, the negative point of those techniques is that they are expensive and may produce further pollution. Compared with other bioprocesses such as adsorption, which is popular because of its high efficiency, accessibility, simplicity, and a vast variety of adsorbent availability [10,11]. Recently, a lot of effort has been put into removing dye from effluent by creating an economical adsorbent with a higher adsorption capacity and no production of harmful chemicals [12,13], Many other bio-adsorbents, including cellulose, rice husks, sawdust, and eucalyptus bark, almond shell, argan nutshells have been described and the agricultural solid wastes have proven their worth in reducing pollution levels [14–17]. In addition, treating wastewater with these adsorbents is a sustainable approach to reducing the buildup of agricultural wastes [18,19] as reported in the study of Ghosh et al. [20] which used agricultural waste materials as eucalyptus leaves for the elimination of crystal violet, coconut coir for removal of safranin-O dye [21] and elimination of malachite green using *Bambusa vulgaris* leaves [22].

Methylene blue (MB) is a synthetic cationic dye with a high degree of chromaticity and good water solubility, making it useful as a chemical indicator, dye, biological stain, and pharmaceutical in many different fields [23];. Nonetheless, the presence of MB in the environment can induce irritation of the eyes and skin, as well as mental disorientation. So, getting rid of MB from polluted water is the most important part of cleaning up waste. Additionally, many batch adsorption experiments successfully reported the removal of MB using a different type of bio-adsorbent such as untreated *Lathyrus sativus* husk [24], untreated and treated *Lathyrus sativus* husk [25] phosphoric acid-activated eucalyptus leaves [26]. These findings demonstrated unequivocally that certain chemical treatments, accountable for the change of functional groups, might enhance the adsorption capabilities of various biosorbents. Therefore, the biosorbents used to remove colors from water require appropriate modification procedures to enhance their adsorption effectiveness [27].

Grapes are the most extensively consumed fruits in the world, which are grown on more than 7.5 million ha of land in 2017 including Algeria, [28]. the sawdust of grapevine wood (GVW) is a naturally occurring common agricultural by-product that is created as a waste product during pruning of vine branches and is made up of organics including cellulose, lignin, hemicellulose, and some other components [29] which can be used as efficient bio-adsorbent [30].

In this study, GVW is utilized as a pristine compound to synthesize sawdust adsorbent, and the yielded product was applied to adsorbing the organic MB from solution media. Also, the adsorption process was studied by isotherms, kinetic analyses, and thermodynamics methods.

2. Materials and methods

GVW materials were provided by a local company and the MB dye (Sigma-Aldrich, Saint Louis, ~70%) (Fig. 1a) was selected in this work as an adsorbate in the adsorption experiments. A solution of MB (10^{-5} mol·L^{-1}) was mixed in deionized water as the standard mixture and then diluted

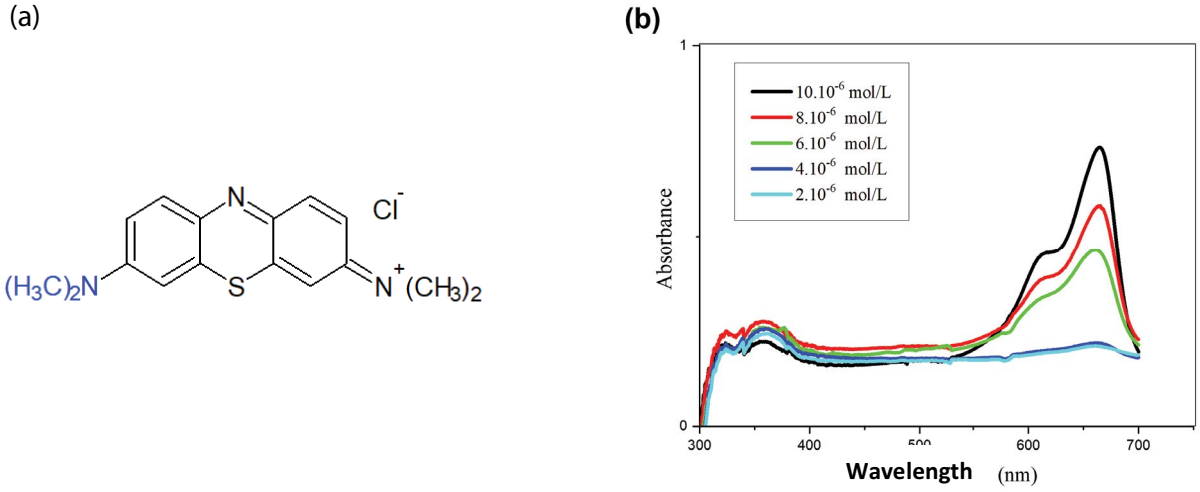

Fig. 1. (a) Chemical bonding of methylene blue. (b) Maximum absorbance wavelength (λ_{max}) of methylene blue at concentrations ranging from 2 × 10^{-6} to 10 × 10^{-6} mol·L^{-1}.

by successive dilution into 2 × 10^{-6} to 10 × 10^{-6} mol·L^{-1}. Concentrated H_2SO_4 (FLUKA, Gillingham, UK, 98.0%) was diluted at 10%. The pH variations were performed using HCl (FLUKA, 37%) and sodium hydroxide NaOH (Sigma-Aldrich, ≥98%) solutions. All the chemical compounds were used in this research without any purification. A PerkinElmer UV-Vis Spectroscopy was employed for recording the absorption data, as a mechanical shaker, and a pH meter (JENWAY 3505, United Kingdom) for pH measurements.

2.1. Determination of methylene blue concentration

The concentrations of dye in the mixture were evaluated by recording the absorbance at the maximum wavelength (λ_{max} = 664.5 nm) (Fig. 1b) and utilizing the calibration curve of dye in the content between 2 × 10^{-6} to 10 × 10^{-6} mol·L^{-1} at pH 6.9 (initial pH), as depicted in Fig. 2.

2.2. Preparation and activation of GVW biosorbent

The GVW materials were provided by Ain Témouchent. They were washed and treated at 105°C for 1 d. The organic agricultural waste was pulverized into 80 μm to 1 mm-sized particle. After that, they were refluxed in H_2SO_4 media at 100°C for 2 h. The obtained grapevine wood activated (GVWA) was rinsed several times with distilled water for removing residual acid and allowed to dry for one day at 105°C after filtering. They were stored at ambient temperature and then used for adsorption studies without further modification.

2.3. Characterization of GVW and GVWA

The oxygen groups of GVW materials were examined using Fourier-transform infrared spectroscopy (FTIR). The composition and morphology of GVW and GVWA were studied using scanning electron microscopy-energy-dispersive X-ray spectroscopy (SEM-EDS). The Brunauer–Emmett–Teller formula was utilized to calculate the surface area. The ASAP 2010-Micromeritics (Germany) device was used to calculate the nitrogen adsorption–desorption characteristics. The structural properties of the samples were examined by X-ray diffraction (XRD; Philips, Netherlands) with a Cuk source.

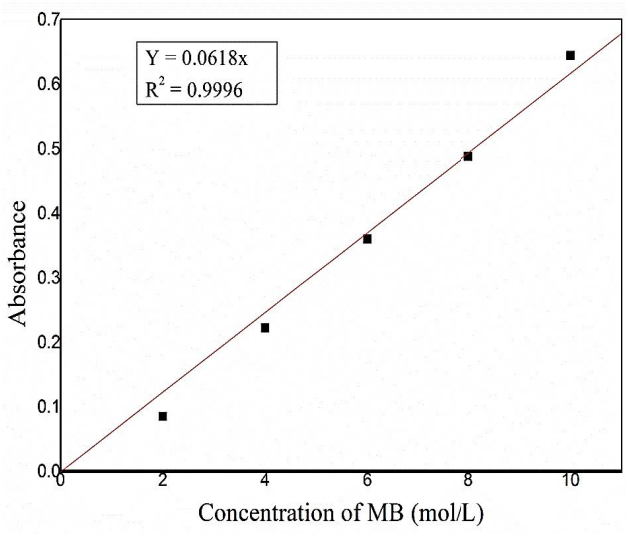

Fig. 2. Calibration plot of methylene blue at a concentration range from 2 × 10^{-6} to 10 × 10^{-6} mol·L^{-1}.

2.3.1. Calculation of the point of zero charges (pH_{pzc})

The pH level of the solution is unaffected by the surface of the grapevine-wood sawdust at pH_{pzc} value [31]. When pH < pH_{pzc}, the positive charge of the sawdust surface favors the adsorption of anionic compounds, and the GVWA surface is negatively charged at pH > pH_{pzc} [32]. The pH_{pzc} of the GVWA samples was characterized via the solid addition technique of Crini and Badot [33]. The initial pH of the mixtures was regulated from 1.67 to 11.2 by mixing 0.15 g of GVWA with 50 mL of 0.01 M NaCl and inserting 0.1 M HCl or NaOH for 48 h. The ultimate pH of the suspensions was determined and measured against the start pH. The pH_{pzc} was obtained by intersecting this curve with the linear plot of $pH_{initial}$ = pH_{final}.

2.4. Adsorption of dye using a batch method

The batch method was used to test the adsorption of 100 mL of MB dye solution on GVWA under different factors, including particle sizes (80/125, 125/250, and 500/1,000 μm), initial MB dye concentrations (10 × 10^{-6} – 30 × 10^{-6} mol·L^{-1}), pH values (2.5–11), temperatures (20°C, 30°C, 40°C and 50°C), shaker speed (100, 500, and 1,000 rpm), contact time (1–180 min) and adsorbent dosage (50–300 mg). The products were refined, and the concentration of MB following the adsorption procedure was determined utilizing UV-Vis Spectroscopy at 664.5 nm.

3. Results and discussion

3.1. Characterization of GVW and GVWA

For a better understanding of the role played by sulfuric acid during the chemical reaction of activation and to pinpoint the functional groups that are connected to them and enable the adsorption actions, FTIR analyses were conducted, and the functional groups of GVW and GVWA before and after adsorption of MB are listed in Table 1.

When comparing the spectra of the raw and activated GVWs (Fig. 3), we found that multiple absorption peaks were observed in the same range but with a reduced intensity of absorption bands. We also noticed that new peaks either appear or disappear with changes in various functional groups.

After sawdust has been activated by sulfuric acid, The intensity of the bands at 1,222.68/1,227.79 cm^{-1} and 1,026.65/1,042.01 cm^{-1} attributed to the C–O bands and the vibration of carboxylic acid C–O bonds, respectively, has increased because the cellulose chains' oxygen-free doublet being protonated and the increased band intensity of asymmetric C–H of the alkyl groups was seen at 2,908.14 cm^{-1}. Due to bonded hydroxyl-OH groups (of carboxyls, phenols, or alcohols) associated with cellulose, lignin, and hemicellulose, the intensity of the large band at 3,336.57/3,341.69 cm^{-1} was reduced [34], which may have been induced by the sulfuric acid's reaction dehydration, which resulted in a

Table 1
Functional groups of raw grapevine wood sawdust and activated grapevine wood determined by the Fourier-transform infrared spectroscopy analysis

Functional groups and mode of vibration	Grapevine wood Before activation	Activated grapevine wood After activation (cm^{-1})	Activated grapevine wood After adsorption (cm^{-1})
C–O–H stretching	3,336.57	3,341.69	3,331.65
Asymmetrical stretching vibration of $–CH_3$ (C sp^3-H)	2,913.06	2,943.78	2,918.72
Symmetrical stretching vibration of $–CH_2$ (C sp^2-H)	–	2,866.25	2,850.70
C=C stretching vibration	–	2,352.04	–
C=O stretching of carboxylic acid	–	1,724.45	–
Stretching vibration of C=C aromatic ring	1,607.42	1,587.67	1,598.75
C=C of aromatic ring	1,507.21	1,512.33	1,510.22
CH_2 deformation	1,450.69	1,456.73	1,453.24
O=S=O stretching vibration		1,362.38	1,316.62
C–O vibration of carboxylic acid	1,222.68	1,227.79	1,229.12
$–SO_3H$ deformation	–	1,160.50	1,157.28
C–O–C stretching	1,026.65	1,042.01	1,029.72
CH out-of-plane deformation	896.14	–	–
S–O stretching	–	900.10	–
N–H deformation	–	728.21	–
C–O–H twist broad	652.14	–	–

no-saturation that revealed a new C=C group and caused the appearance of the latter band at 2,352 cm^{-1} [35]. Also, a decrease in the GVWA band's 1,607.42/1,587.67 cm^{-1} intensity was assigned to C=C skeletal vibration of the condensation aromatic system [36], and this might be brought on by a drop in lignin content.

Furthermore, the new strong vibration bands of C=O from the carboxylic group and C=C of ketones, aldehydes, or carboxylic groups centered around 1,724.45 and 2,352.04 cm^{-1} appeared with the observation of another peak at 728.77 cm^{-1} for out-of-plane of NH and, a minor peak at 2,866.25 cm^{-1} for symmetrical CH of the alkyl chains. The disappearance of the band at 652.42 cm^{-1} is indicative of the twist C–O–H in the raw GVW spectra [37]. According to the infrared spectra, this change in absorption bands and intensity may be proof that the GVW has been chemically activated.

The data of the FTIR analysis revealed that there were multiple carboxylic acid absorption peaks and intermolecular hydrogen bonds of –OH, pointing to the material's complexity and the potential active sites for interacting with the cationic MB. The spectra of GVWA following MB adsorption are revealed in Fig. 3b, and it can be indicated that the majority of oxygen groups were affected [38], as well as the absence of the peaks at 1,724.45 and 2,352.04 cm^{-1}. The largest changes were seen in the following measurements: 3,341.69–3,331.65 cm^{-1}; 2,943.78–2,918.72 cm^{-1}; 1,587.67–1,598.75 cm^{-1}; 1,512.33–1,510.22 cm^{-1}; 1,456.73–1,453.24 cm^{-1}; 1,362.38–1,316.62 cm^{-1}; and 1,227.79–1,229.12 cm^{-1}, 1,160.50–1,157.28 cm^{-1}; and 1,042.01–1,029 cm^{-1}.

The FE-SEM and energy-dispersive X-ray spectroscopy (EDX) were illustrated to present the shape, and morphology of the GVW before and after activation, as presented in Figs. 4 and 5. The highly anisotropic nature of the SEM image of GVW before sulfonation (Fig. 4a) was primarily caused by the spatial orientations of the natural constituents of wood, and the SEM image of the GVW sample after the chemical treatment with sulfuric acid revealed well-appeared pores and micro-sized particles generated. It's possible that the substantial sulfonation was the cause of the particles' rough surface. The same conclusions were reached in recent studies for biosorbents from *Pinus sylvestris* [39]. According to the EDX analysis of activated GVW (Fig. 5b), the oxidation process that may have created the oxygen groups on the GVW resulted in greater oxygen levels in the activated GVW sawdust.

As exhibited in Fig. 6, the XRD profile of GVW sawdust untreated showed the presence of significant 2θ angle peaks at 15.37°, 23.71° and, 35.03°, corresponding, respectively to the diffraction planes 101, 002, and 040 [40], relative to the natural native cellulose I structure of lignocellulosic materials, since there was no doublet in the main peak at 2θ = 23.71°, with low crystallinity (amorphous) corresponding to an irregular structure. The GVW untreated presents a large amorphous portion because of its high lignin amount [41,42]. After chemical activation, the diffraction intensity of these peaks increased dramatically, with a displacement in the position at lower angles (15.25°, 22.35°, 34.35°), which resulted in an improvement in the crystallinity of the cellulose. To confirm these results, the crystallinity index of raw GVW and GVWA was calculated according to Eq. (3) [40].

$$\mathrm{Cr}_I = \left(\frac{\left(I_{002} - I_{\mathrm{Am}}\right)}{I_{002}} \right) \times 100 \quad (1)$$

The crystallinity values were estimated as 51.84% and 71.93% for the untreated GVW and treated GVW, respectively. A remarkable increase in the number of crystallinity regions of treated GVW was because of the partial elimination of the amorphous phases of lignin and

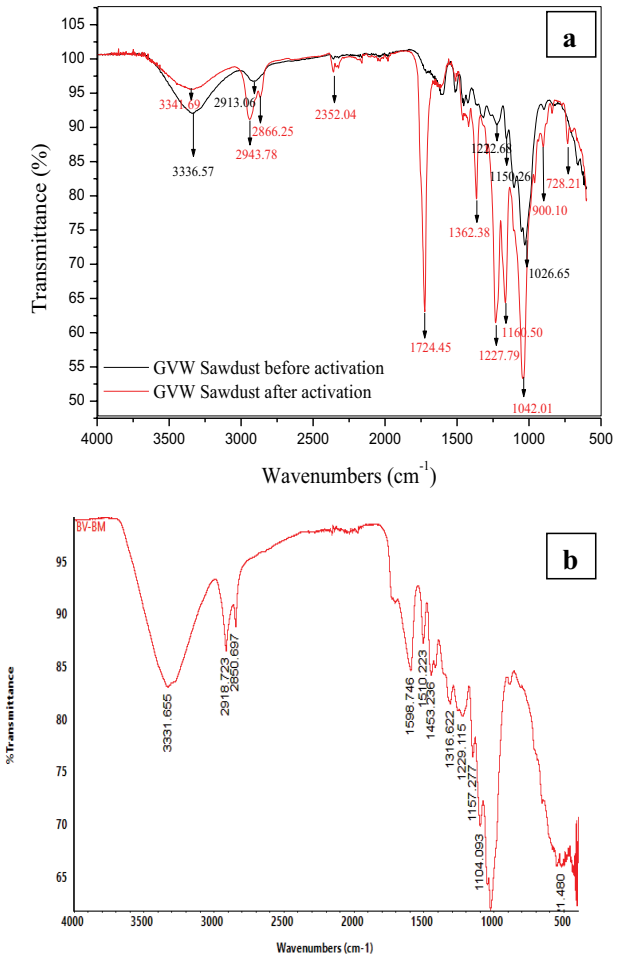

Fig. 3. Fourier-transform infrared spectroscopy profiles of: (a) grapevine wood sawdust before and after chemical activation (GVWA) and (b) activated grapevine wood after adsorption of methylene blue.

hemicelluloses during chemical treatment. These observations have also been reported [43,44]. So, we found that the activation process was done well.

Figs. 7 and 8 show the surface area and pore diameter distribution of raw GVW, as assessed by the N_2 sorption isotherm at 77 K Brunauer–Emmett–Teller (BET technique) [44]. Concerning mesoporous material, the isotherms for GVW are primarily type IV shapes with clearly marked H_3 hysteresis loops (Fig. 7a and b). Since the majority of the pores had a diameter larger than 20 and fewer than 500, following IUPAC categorization, Fig. 8a and b imply the mesoporosity of raw GVW and activate GVW. Raw GVW and GVWA were determined to have BET surfaces of 0.5873 and 1.6319 $m^2 \cdot g^{-1}$, respectively. The dissociation and dispersion of H_2SO_4 into the pores, which were improving the pore density on its surface, were thought to be the causes of GVWA's greater surface area. Because of its larger surface area (Table 2), GVWA was a suitable and advantageous adsorbent for the adsorption of MB. These results align with other raw sawdust mentioned in the literature [45,46,24].

The graph (Fig. 9) showed that the pH_{pzc} of the GVWA sawdust (after Sulfonation) was found to be around 5, which reveals the acid character of the GVWA because of the treatment with H_2SO_4. According to these findings, the grapevine wood sawdust will be suitable for removing MB at pH > pH_{pzc}. Another researcher noted a similar finding after the treatment of biomass materials with H_2SO_4 such as mango peel (pH_{pzc} = 4.6) [47].

3.2. Adsorption studies

Fig. 10 demonstrates the impact of GVWA particle size on the dynamics of dye adsorption in solutions. It should be noted that the activated GVW's ability to remove dye is less effective as particle size increases because of the smaller surface area of larger particle sizes, which leaves the biosorption process with fewer active sites. However, these small, tiny particles may block percolation systems or be

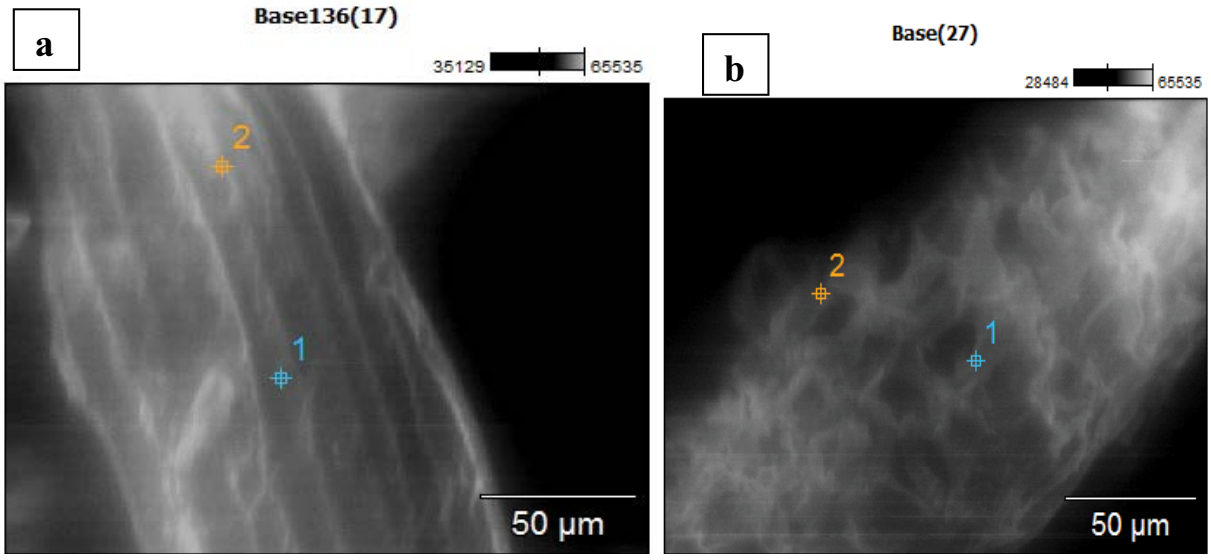

Fig. 4. Scanning electron microscopy image of (a) grapevine wood and (b) activated grapevine wood sawdust.

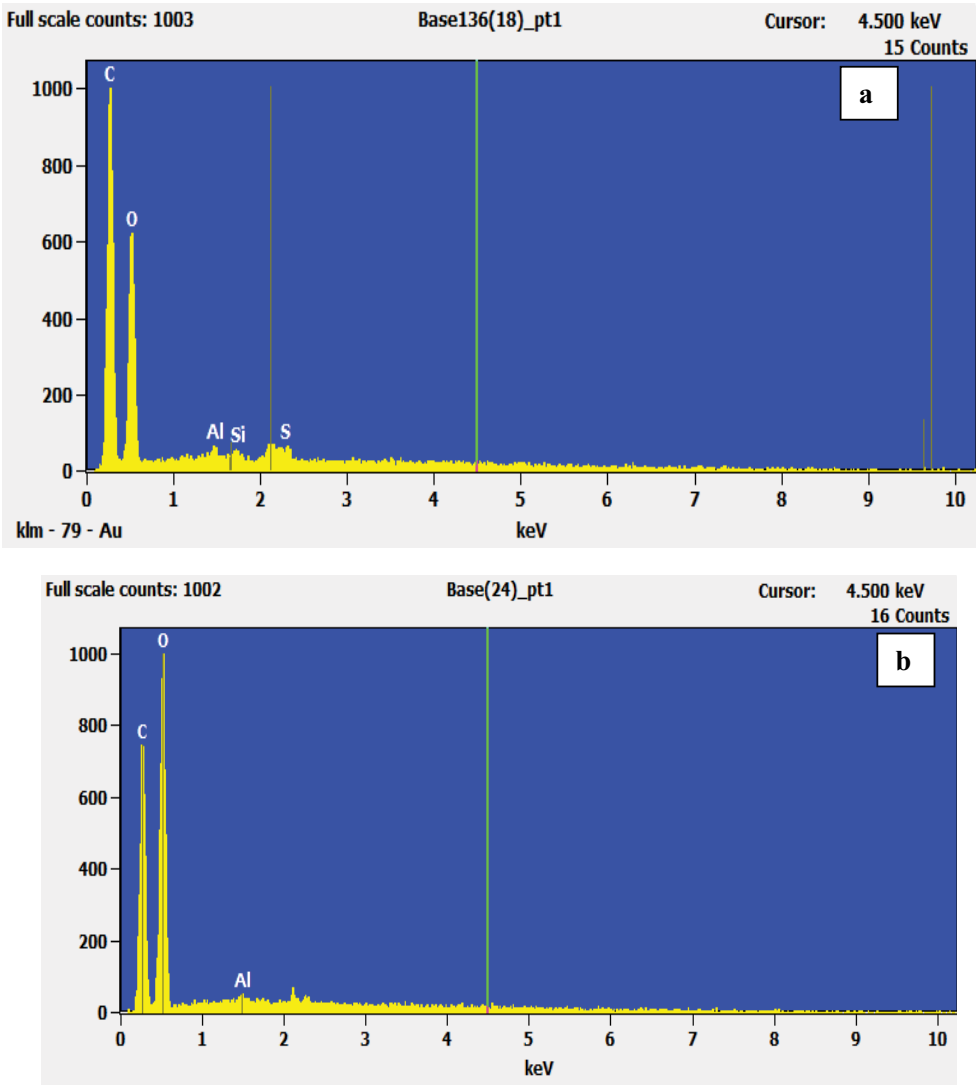

Fig. 5. Energy-dispersive X-ray spectroscopy image of (a) grapevine wood and (b) activated grapevine wood sawdust.

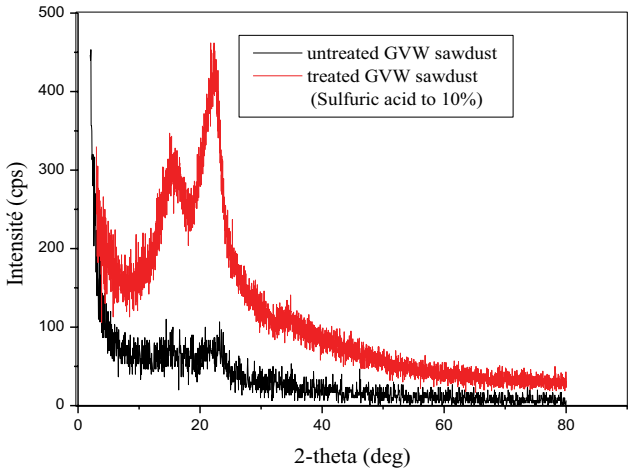

Fig. 6. X-ray diffraction profiles of grapevine wood samples before and after activation (GVWA).

difficult to recover [48]. As a result, we chose particles with a d = 125/250 μm size. Various studies came to the same conclusions [49,50].

As shown in Fig. 10b, the change in activation GVW mass (from 50 to 300 mg) results in a considerable difference in the elimination of MB (10^{-5} mol/L). The findings indicate that as the dosage is increased, the GVWA sawdust's adsorption effectiveness increases as a result of an increment in the adsorbent's active centers [51]. An optimal percentage removal (99.85%) was accomplished with 100 mg of GVWA sawdust. A maximum percentage removal (99.85%) was accomplished with 100 mg of GVWA sawdust. Other researchers reported similar findings [52,53].

According to Fig. 10c, the 10×10^{-6} to 30×10^{-6} mol·L^{-1} BM adsorption process from 100 mL of solution with a particle size of 125/250 μm started out rapidly and took between 50 and 120 min to reach equilibrium. At 180 min, it was discovered that the maximum amount of dye adsorbed was 9.88×10^{-3}–29.95×10^{-3} mmol·g^{-1} (98.86%–99.82% removal

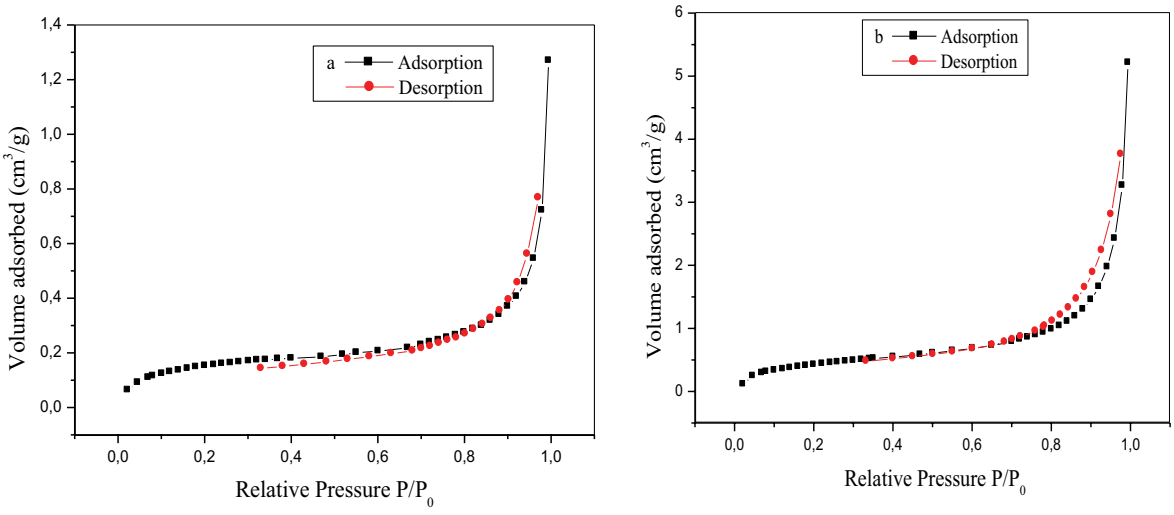

Fig. 7. N_2 adsorption–desorption isotherms at 77 K of (a) grapevine wood and (b) activated grapevine wood.

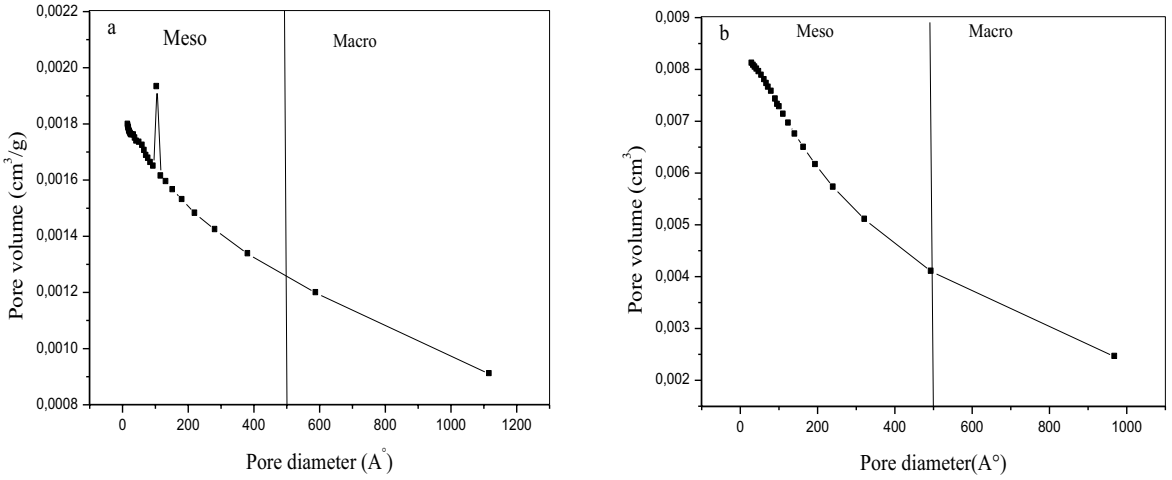

Fig. 8. Pore-size distribution plot based on Barrett–Joyner–Halenda model of (a) grapevine wood and (b) activated grapevine wood.

Table 2
Nitrogen sorption results of grapevine wood and activated grapevine wood

Samples	Brunauer–Emmett–Teller method		Barrett–Joyner–Halenda method		
	S_{BET} ($m^2 \cdot g^{-1}$)	V_{TOTAL} ($cm^3 \cdot g^{-1}$)	S_{Meso} ($m^2 \cdot g^{-1}$)	V_{Meso} ($cm^3 \cdot g^{-1}$)	d_{Meso} (Å)
Grapevine wood sawdust	0.5873	0.00019	0.2911	0.00179	246.935
Activated grapevine wood sawdust	1.6319	0.00061	1.3176	0.00771	234.057

efficiency), which indicates the adsorption–desorption equilibrium [54].

The original concentration of dye BM effect: 100 mg of GVW was introduced to different initial concentrations of dye solution (10×10^{-6} to 30×10^{-6} mol·L^{-1}) and stirred for 180 min at 293 K to study the MB concentration impact on the adsorption dynamic Fig. 10 demonstrates that the biosorption capacity of activated GVW sawdust may increase with an increase in the initial concentration of MB even though the concentration did not reach equilibrium, showing that the increased initial MB increased the driving force between dye and adsorbents [55]. Other researchers have reported comparable results for the MB removal via H_2SO_4 treatment of coconut [56] and mango [57].

100 mg of GVW was introduced to the MB solution with initial doses (10^{-5} mol/L) with various pH ranges from 2.5 to 11 at a fixed stirring speed for 180 min at 293 K. According to Fig. 11a, the dye adsorption increases from 84.50% to 93.63% as the solution pH rises because the ionization of activated GVW causes the positive charges adsorbent

(MB^+) and the negatively charges adsorbent surface to become more electrostatically attracted ($pH > pH_{pzc}$) in an alkaline condition. The activated GVW sawdust surface has a high concentration of H^+ ions, which reduces the dye adsorption capability even if the adsorbent surface is positively charged in acidic pH ($pH < pH_{pzc}$) [58]. This finding indicates that the MB was predominantly adsorbed as MB^0 [22]. The pH value of 6.9 was determined from the experimental results to be the best for MB dye adsorption in future research. The findings of Uddin and Nasar [59] are in agreement with this.

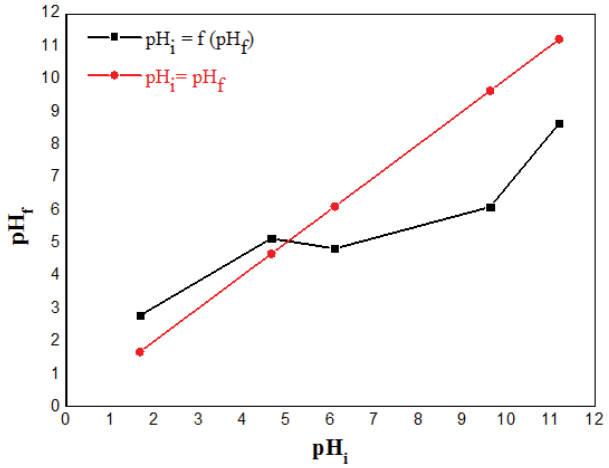

Fig. 9. Point of zero charge of activated grapevine wood.

One of the most important factors that can influence pollutant adsorption behavior is temperature [60]. At 20°C, 30°C, 40°C, and 50°C, the temperature-dependent adsorptions were carried out by adding 100 mg of the adsorbent to 100 mL of the MB suspension (Fig. 11b). When the temperature was raised, it was discovered that the percent removal reduced from 99.85% to 97.71%, and this may be due to the decrease of active centers on the surface [61,62].

The adsorption effectiveness is also significantly impacted by the shaker speed. The impact of stirrer speed was investigated at various speeds between 100 and 1,000 rpm while maintaining all experimental conditions. As shown in Fig. 11c, when the speed is raised and the time needed to reach equilibrium is decreased, the removal efficiency rises from 98.40% to 99.64%. o, the fact that biosorbents don't stick together means that more biomass surface area is available, which leads to the fast adsorption of MB [63,64].

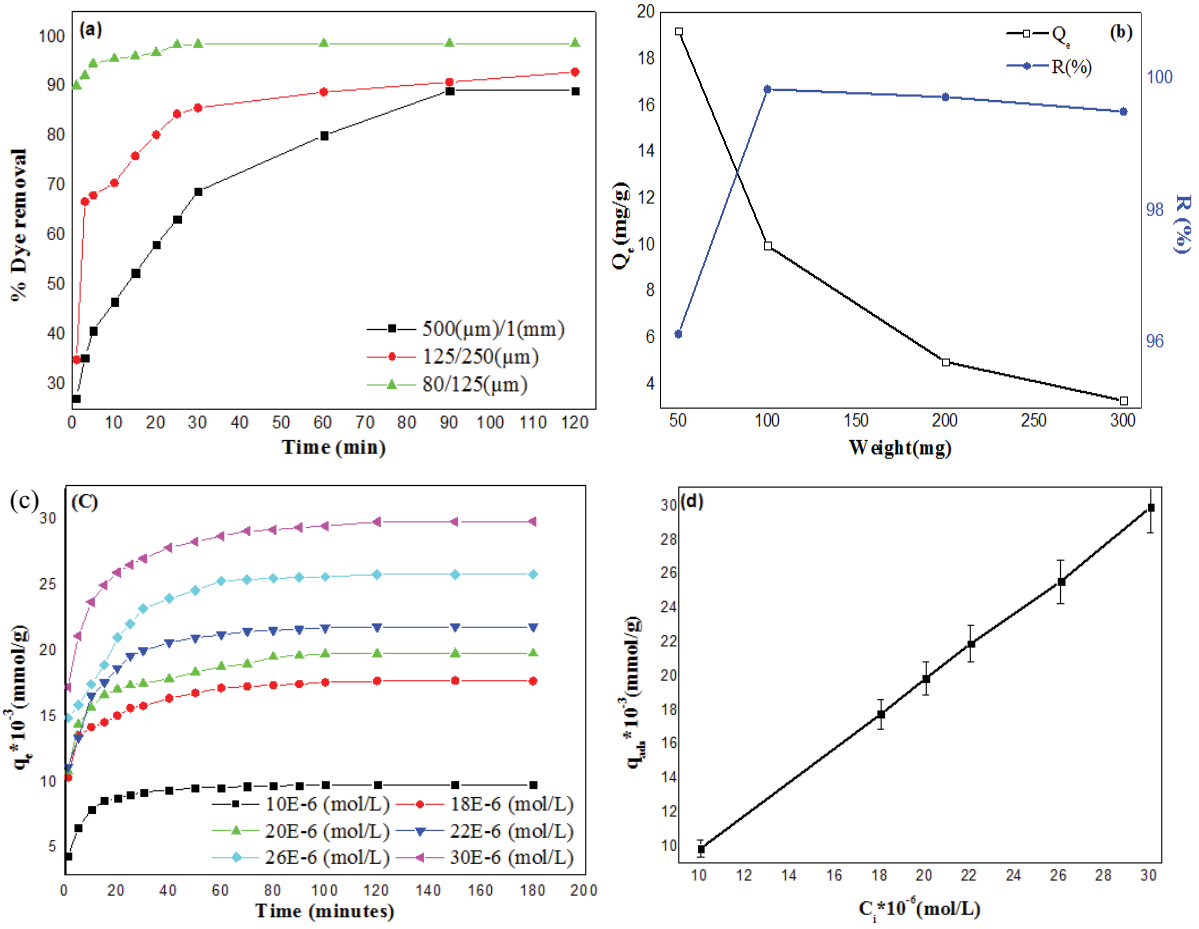

Fig. 10. Impact of (a) particle size, (b) adsorbent dose, (c) contact time and (d) initial concentration on the kinetics of methylene blue dye adsorption onto activated grapevine wood.

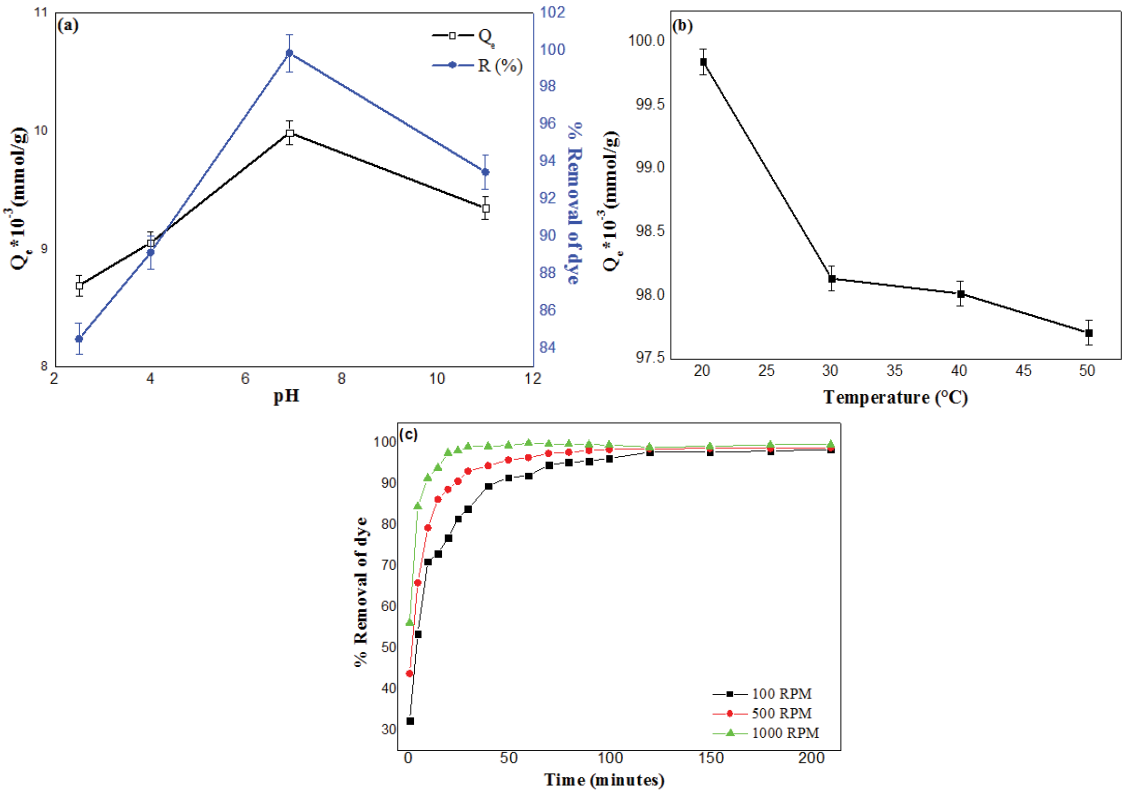

Fig. 11. Effect of the (a) pH, (b) temperature and (c) shaker speed on the kinetics of methylene blue dye adsorption onto activated grapevine wood.

3.3. Theoretical study

3.3.1. Kinetic modeling of BM sorption onto GVWA sawdust

There are several stages involved in the sorbate's passage from the liquid phase to the biosorbent's surface, which can be used as speed control mechanisms, according to biosorption kinetics, which defines the method of MB elimination. With fixed parameters, the kinetics modeling of GVWA sawdust adsorption behaviors toward various initial concentrations of MB solution (10^{-5} – 3×10^{-5} mol·L^{-1}) has been reported using kinetic rate:

The adsorption dynamics data in a system were calculated from Lagergren's pseudo-first-order model [65] by the following integral equation:

$$\ln\left(Q_e - Q_t\right) = \ln Q_e - K_1 t \tag{2}$$

where Q_e and Q_t: the instant and equilibrium amount of adsorbed MB (mmol·g^{-1}); K_1: the equilibrium rate constant of pseudo-first-order kinetics (min^{-1}). K_1 and Q_e values were obtained using the slope and intercept of $\ln(Q_e - Q_t)$ vs. t of linear plots (Fig. 12) as given in Table 3.

As shown in Fig. 13 and Table 4, Blanchard's pseudo-second-order integral equation is as follows [66]:

$$\frac{t}{Q_t} = \frac{1}{K_2 Q_e^{\,2}} + \frac{1}{Q_e} t \tag{3}$$

where K_2 signifies the second-order rate constant (g·mmol^{-1}·min^{-1}) and h: the initial sorption rate as follows:

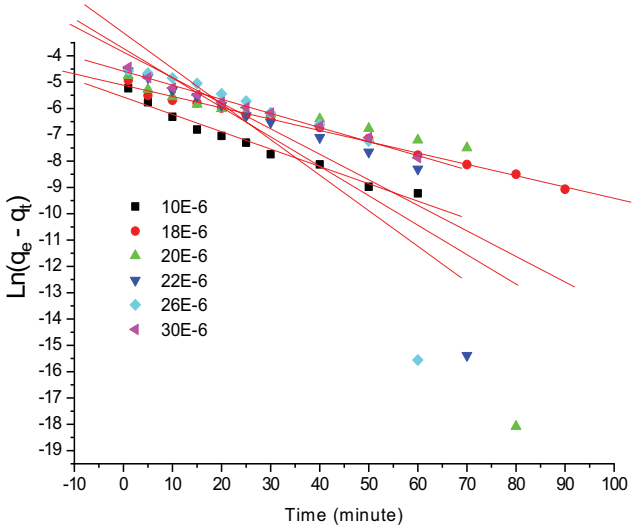

Fig. 12. Pseudo-first-order kinetic curves for the adsorption of the dye onto activated grapevine wood.

$$h = K_2 Q_e^2 \tag{4}$$

3.3.1.1. Intraparticle diffusion model

To explore the adsorption mechanism, Weber and Morris' intraparticle diffusion model [67] was utilized. The intraparticle equation is presented in its linear version as follows:

Table 3
Pseudo-first-order kinetic parameters for adsorption of methylene blue onto activated grapevine wood by linear and non-linear regression analysis method

C_0 (mol/L)	K_1 (mmol·g^{-1}·min^{-1})	$Q_{e\,exp}$ (mmol·g^{-1})	$Q_{e\,cal}$ (mmol·g^{-1})	R^2	ARE %
Linear regression					
10 × 10^{-6}	6.59E-02	9.77E-03	3.83E-03	0.9722	3.577
18 × 10^{-6}	4.30E-02	1.77E-02	6.01E-03	0.9918	3.8802
20 × 10^{-6}	9.71E-02	1.96E-02	2.11E-02	0.5178	0.4592
22 × 10^{-6}	1.12E-01	2.15E-02	2.43E-02	0.7264	0.7583
26 × 10^{-6}	1.35E-01	2.54E-02	4.40E-02	0.6496	4.3189
30 × 10^{-6}	5.36E-02	2.92E-02	1.03E-02	0.9890	3.8155
Non-linear regression					
10 × 10^{-6}	2.91E-01	9.77E-03	9.471E-03	0.9321	0.1776
18 × 10^{-6}	9.55E-01	1.77E-02	1.646E-02	0.9065	0.3969
20 × 10^{-6}	4.53E-01	1.96E-02	1.869E-02	0.9071	0.2748
22 × 10^{-6}	2.73E-01	2.15E-02	2.096E-02	0.9178	0.1579
26 × 10^{-6}	2.87E-01	2.54E-02	2.433E-02	0.9166	0.2465
30 × 10^{-6}	6.06E-01	2.92E-02	2.847E-02	0.9035	0.1457

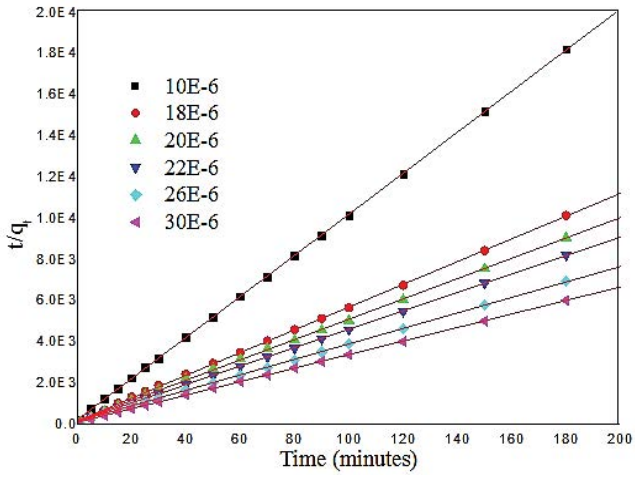

Fig. 13. Pseudo-second-order kinetics curves for the adsorption of the methylene blue onto activated grapevine wood.

$$Q_t = K_i t^{1/2} + C \tag{5}$$

where K_i is the intraparticle diffusion rate constant (mmol·g^{-1}, min$^{-1/2}$), and C is the constant that indicates the thickness of the boundary layer (mmol·g^{-1}).

The intraparticle diffusion rate constant (K_i and correlation coefficient (R^2) can both be determined from the slope of the graph Q_t vs. $t_{1/2}$ to determine the model's fitness [67]. The findings are exhibited in Fig. 14 and Table 5 for the varied initial concentrations.

3.3.1.2. Error functions

The correlation coefficients (R^2) and average relative error (ARE) were utilized to validate the models suggested to show the adsorption isotherms. Eq. (10) was used to determine the ARE [68]:

$$\text{ARE}\% = \frac{100}{n}\sum_{i=1}^{n}\left|\frac{Q_{e\,exp} - Q_{e\,cal}}{Q_{e\,exp}}\right| \tag{6}$$

With $Q_{e\,exp}$ and $Q_{e\,cal}$ represent the experimental and theoretical values of the content of dye adsorbed at equilibrium, respectively, and n is the number of experimental data.

The graph $\ln(Q_e - Q_t)$ vs. t is not linear, and the estimated adsorption capacity (Q_e) did not match the experimental values, as shown in Fig. 12 which confirms that the adsorption of dye onto GVWA did not follow the pseudo-first-order equation as found it by other investigations [56,69]. Additionally, the pseudo-second-order kinetic model's fit to the experimental data at the various initial concentrations is shown in Fig. 13, which exhibits a linear relationship with an intercept very close to zero and the theoretical numbers estimated by the pseudo-second-order model ($Q_{e\,cal}$) match the experimental data ($Q_{e\,exp}$), as shown in Table 4. Furthermore, a strong fit between the experimental and computed data was indicated by the high correlation coefficient values (~0.99) and the lower value of ARE. These results demonstrate that the pseudo-second-order kinetics model describes MB adsorption over GVWA sawdust. The same results were indicated by El Messaoudi et al. [24]. Table 4 further demonstrates that the values of the K_2 decrease and the h value increases as the initial concentration of MB increases, which may be attributed to the better driving force at higher concentrations. Zhu et al. [36] and Hasani et al. [71] both observed similar findings. The experimental data was an excellent fit for the pseudo-second-order kinetics model, as shown by the findings of the non-linear method shown in Tables 3 and 4. Additionally, it was noted that when compared to linear forms, the average relative error (ARE) of non-linear forms showed a

Table 4
Pseudo-second-order for adsorption of dye onto activated grapevine wood by linear and non-linear regression analysis method

C_0 (mol/L)	K_2 (mmol·g^{-1}·min^{-1})	$Q_{e\,exp}$ (mmol·g^{-1})	$Q_{e\,cal}$ (mmol·g^{-1})	h (mmol·g^{-1}·min^{-1})	R^2	ARE %
Linear regression						
10 × 10^{-6}	4.45E+01	9.77E-03	1.00E-02	4.47E-03	0.9999	0.1553
18 × 10^{-6}	1.85E+01	1.77E-02	1.81E-02	6.05E-03	0.9999	0.1490
20 × 10^{-6}	1.48E+01	1.96E-02	2.03E-02	6.08E-03	0.9999	0.1989
22 × 10^{-6}	1.47E+01	2.15E-02	2.24E-02	7.36E-03	0.9999	0.2236
26 × 10^{-6}	9.58E+00	2.54E-02	2.66E-02	6.78E-03	0.9997	0.2826
30 × 10^{-6}	1.13E+01	2.92E-02	3.04E-02	1.05E-02	0.9999	0.2470
Non-linear regression						
10 × 10^{-6}	5.60E+01	9.77E-03	9.88E-03	5.47E-03	0.9714	0.0687
18 × 10^{-6}	6.62E+01	1.77E-02	1.750E-02	2.03E-02	0.9153	0.0503
20 × 10^{-6}	4.84E+01	1.96E-02	1.91E-02	1.76E-02	0.922	0.1638
22 × 10^{-6}	2.49E+01	2.15E-02	2.16E-02	1.16E-02	0.8978	0.0115
26 × 10^{-6}	2.27E+01	2.54E-02	2.50E-02	1.42E-02	0.782	0.0843
30 × 10^{-6}	4.31E+01	2.92E-02	2.89E-02	3.61E-02	0.9040	0.0530

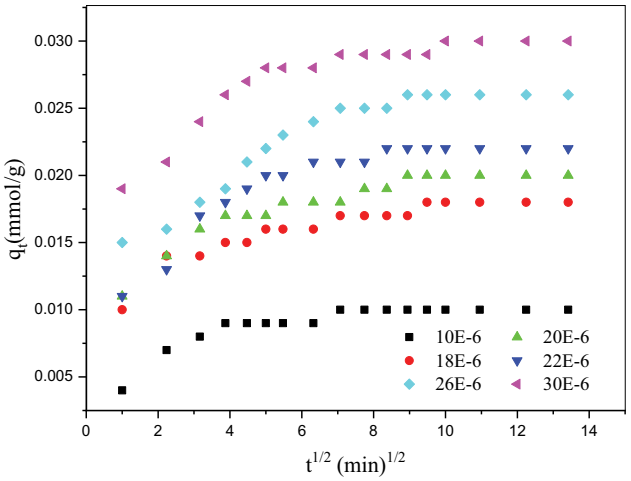

Fig. 14. Intraparticle diffusion kinetics plots.

lower value. According to Fig. 14, there are three steps in the MB adsorption process, and the intraparticle diffusion is provided with three sequential linearities. The first sharp part is concerned with the extremely rapid adsorption of Vinewood sawdust onto the exterior surface. The second area is the longest stage in the diffusion of the MB molecules via the adsorbent's pores. According to Fig. 15 and Table 4, this diffusion model's R^2 values were closer to 1 (0.94–0.99), and the second-stage's linear lines representing each concentration level did not all go through the origin.

3.3.2. Adsorption isotherms models

The sorbent's isotherm properties may reveal information on its surface characteristics and affinity as well as the adsorption mechanism [72]. Adsorption by Langmuir isotherm implies that adsorption will take place on a monolayer surface with well-defined adsorption sites and no dye molecule interaction. The following linear equation [73] illustrates the non-linear Langmuir equation:

$$\frac{1}{C_e} = K_L Q_m \frac{1}{Q_e} - K_L \tag{7}$$

The values of Q_m and K_L are shown in Table 4 after being calculated from the intercept and slope of the linear plot of $1/C_e$ vs $1/Q_e$ (Fig. 16a).

The dimensionless constant separation factor (R_L) of Hall, provided by the formula below [74], was used to represent the fundamental properties of the Langmuir isotherm:

$$R_L = \frac{1}{1 + K_L C_0} \tag{8}$$

According to Freundlich adsorption isotherm, adsorption involves interactions between adsorbed molecules and multilayer adsorption on a heterogeneous surface [75], and the heat of adsorption falls exponentially with the rate of solid surface saturation, which is given by the non-linear equation as follows [76]:

$$\ln Q_e = \ln K_F + \frac{1}{n} \ln C_e \tag{9}$$

The values of n and K_F were estimated from the slope and intercept obtained from plotting $\ln(Q_e)$ vs. $\ln(C_e)$ (Fig. 16b).

The Temkin adsorption isotherm model was designed to explain adsorption with the assumption that, during adsorption in the gas phase, the heat of adsorption of all molecules in the layer drops linearly due to indirect adsorbate/adsorbate interactions [77,78].

The linearized form of the isotherm of the Temkin equation is given as:

$$Q_e = B_T \ln K_T + B_T \ln C_e \tag{10}$$

Table 5
Intraparticle diffusion kinetic parameters for adsorption of methylene blue onto activated grapevine wood by linear and non-linear regression analysis method

C_0 (mol/L)	$Q_{e\,exp}$ (mmol·g^{-1})	$Q_{e\,cal}$ (mmol·g^{-1})	K_i	C	R^2	ARE %
Linear method						
10 × 10^{-6}	9.77E-03	9.704E-03	3.393E-04	0.00667	0.5972	0.0371
18 × 10^{-6}	1.77E-02	1.765E-02	5.201E-04	0.01245	0.7836	0.0001
20 × 10^{-6}	1.96E-02	1.905E-02	6.171E-04	0,01353	0.7869	0.1671
22 × 10^{-6}	2.15E-02	2.073E-02	7.762E-04	0.01424	0.7016	0.2195
26 × 10^{-6}	2.54E-02	2.395E-02	9.553E-04	0.01655	0.8169	0.3346
30 × 10^{-6}	2.92E-02	2.843E-02	7.710E-04	0.02198	0.7230	0.1537
Non-linear method						
10 × 10^{-6}	9.77E-03	9.5708E-03	3.2097E-04	0.0067	0.6111	0.1175
18 × 10^{-6}	1.7E-02	1.3069E-02	4.9854E-04	0.01257	0.7909	0.1527
20 × 10^{-6}	1.96E-02	1.8946E-02	5.9439E-04	0.01363	0.7822	0.1979
22 × 10^{-6}	2.15E-02	2.0584E-02	7.5946E-04	0.01423	0.7238	0.2605
26 × 10^{-6}	2.54E-02	2.3493E-02	9.480E-04	0.01615	0.799	0.4403
30 × 10^{-6}	2.92E-02	2.8404E-02	7.6537E-04	0.022	0.7062	0.1591

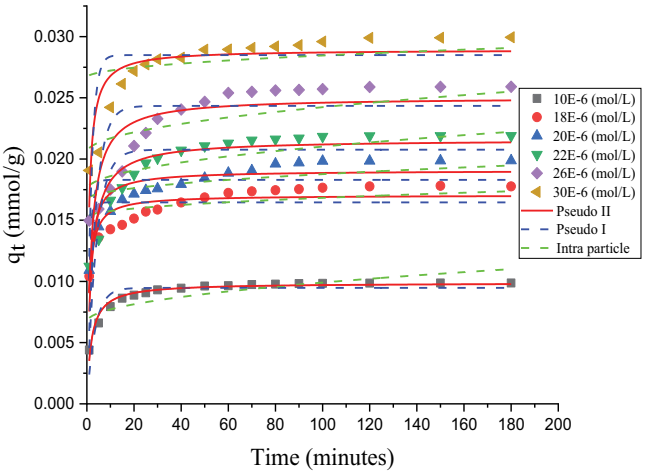

Fig. 15. Adsorption kinetics models non-linear of methylene blue onto activated grapevine wood

With:

$$B_T = \frac{R_T}{b_T} \tag{11}$$

where B_T is the Temkin constant (J·mol^{-1}), T present the absolute temperature (K), R is the gas constant (8.314 J·mol^{-1}·K^{-1}), K_T is empirical Temkin isotherm constant (L·mg^{-1}). The slope and intercepts of the plot of Q_e vs. ln(C_e) (Fig. 16c) were used to calculate the B_T and K_T and presented in Table 6.

Experiment data fitting analysis showed that the Langmuir isotherm provided the best linear and non-linear fits which indicated the uniform energies of adsorption onto the surface and no transmigration of adsorbate in the plane of the surface as reported by Ahmed et al. [79]. The existence of a primary monolayer adsorption behavior on the produced biosorbent was supported by the greatest correlation coefficient adsorption of MB values closer to unity (R^2 = 0.9846) and lower average relative error. The isotherm's type is defined by the value of R_L; if 0 < R_L < 1, the isotherm is favorable, unfavorable (R_L > 1), linear (R_L = 1), or irreversible (R_L = 0). As shown in Table 4 and Fig. 17, the R_L values are larger than 0 and less than 1, and they decrease when the initial concentration is increased. As a result, the MB's adsorption process onto the GVWA sawdust is successful. Identical findings were also reported by Ghosh et al. [80].

The maximal adsorption capacity of MB on GVWA sawdust was 0.6894 mmol·g^{-1} (equivalent 220.51 mg·g^{-1}) and was compared to several adsorbents published in the literature (Table 7).

Table 7 compares the maximum adsorption capacity (q_{max}) of MB obtained for GVWA with those of other natural biosorbents. It can be seen that the adsorption capacity of MB on GVWA is higher than that of most of the other low-cost adsorbents motioned, indicating that GVWA was very promising and environmentally friendly. Furthermore, GVWA are reported as low-cost due to the usage of waste materials with simple method of modification because the classification of adsorbents as waste byproducts or engineered adsorbents would be reflected more by their source and cost [94]. There are financial and ecological benefits to be gained from used agricultural waste [95], then the utilization of an adsorbent is an important element that should be studied in order to make more accurate predictions about the adsorbent's lifecycle and developed in optimal regeneration methods [96].

3.4. Thermodynamics analysis

To establish the thermodynamic characteristics of GVWA sawdust, the adsorption procedure was tried at various temperatures, as shown in Fig. 18. MB adsorption's

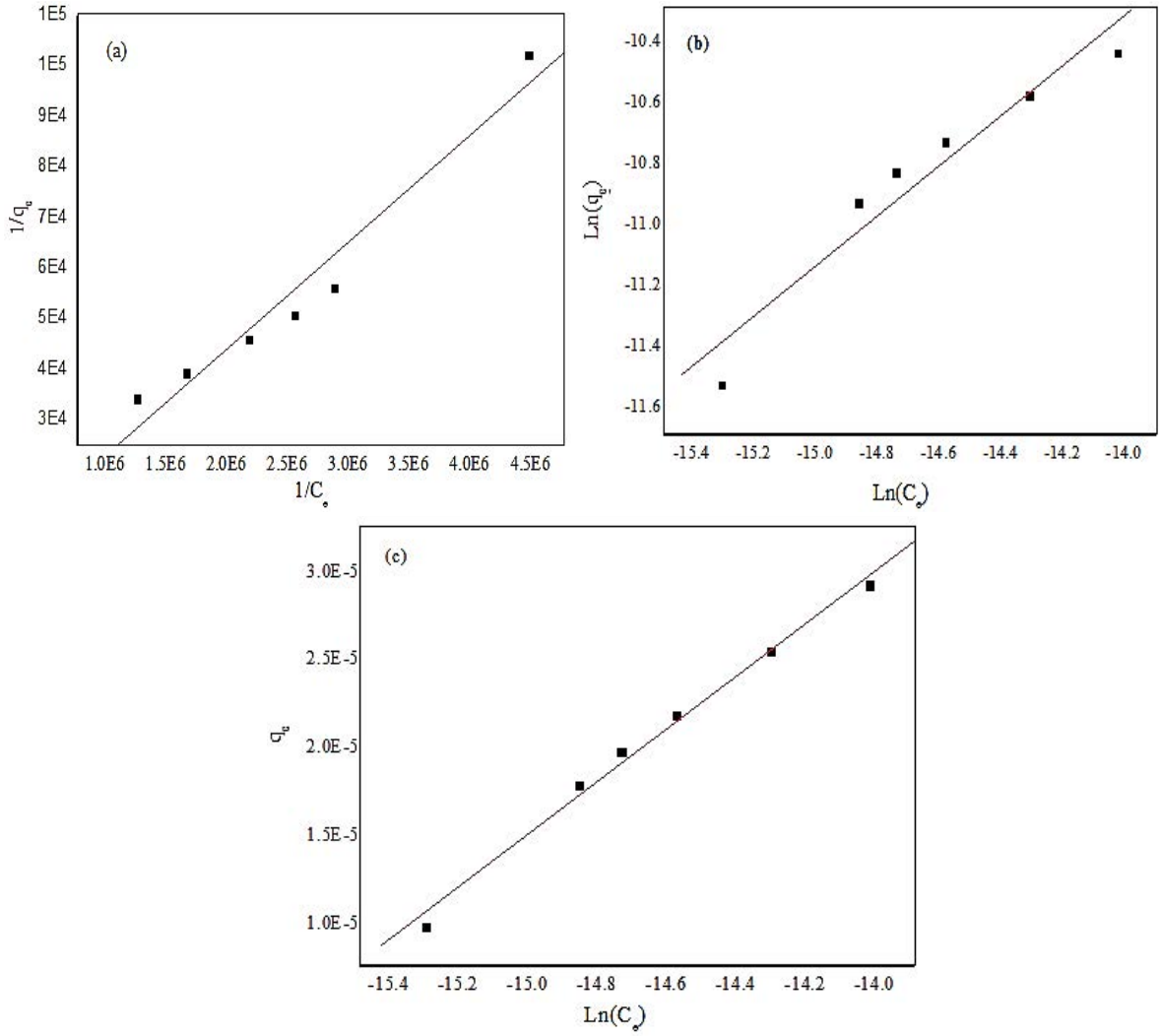

Fig. 16. Linear plot of (a) Langmuir, (b) Freundlich and (c) Temkin isotherm for adsorption of dye onto activated grapevine wood.

thermodynamic variables were calculated using van't Hoff equation and the Gibbs free energy [97].

$$\Delta G^\circ = -RT\ln K_d \tag{12}$$

According to Gibbs' free energy equation:

$$\Delta G^\circ = \Delta H^\circ - T\Delta S^\circ \tag{13}$$

Combining Eqs. (20) and (21), we get:

$$\ln K_d = \frac{\Delta S^\circ}{R} - \frac{\Delta H^\circ}{RT} \tag{14}$$

Values for ΔH° and ΔS° obtained from van't Hoff plots' slope and intercept are summarized in Table 8.

Table 8 indicated that the solid/solution border increased during the adsorption process, and the negative value of enthalpy ΔH° indicates that the removal of MB on GVWA sawdust is exothermic in nature. According to the research, the usual free energy variation for physisorption ranges from –20 to 0 kJ·mol^{-1}, while the variation for chemisorption ranges from 80 to 400 kJ·mol^{-1} [98], the negative ΔG° values, which ranged from –9.77 to –7.77 kJ·mol^{-1} which suggests that the physisorption is a mechanism proposed to explain the adsorption reaction investigated here. Dbik et al. [99] were able to reach a similar finding in their research. . The rise in ΔG° with temperature suggests that high-efficiency adsorption occurs at low temperatures. Aichour et al. [62] achieved a related observation.

3.5. Adsorption mechanisms of methylene blue

The experimental results of the influence of the pH on the adsorption equilibrium of MB demonstrated that alkaline pH (pH > pH_{pzc}) was suitable for cationic dye adsorption and was not favored in the acidic pH. However, at higher pH (6.9–11), previous FTIR analyses showed that the cationic MB^+ was the dominant species (positively charged nitrogen or sulfur on MB), which was electrostatically drawn to the negatively charged (anionic groups) of

the GVWA surface. These groups, which were all moved following adsorption, included hydroxyl (OH), carboxyl (COOH), carbonyl (C=O), and sulfonic (SO_3H). On the other hand, when pH (pH < pH_{pzc}) was between 2.5 and 4, electrostatic interactions did not favor adsorption, but the GVWA demonstrated a good capacity for MB adsorption, indicating that MB's adsorption mechanisms were not limited to electrostatic attraction. With lowering solution pH levels of 2.5 to 4, the MB molecule was the neutral species MB° [46], but the surface of GVWA was ionized (positively charged). from these test conditions, it is conceivable to explain the adsorption of MB can be related to π–π dispersive interactions between the π-electrons of the aromatic rings of the MB and the π-electrons from the aromatic rings of GVWA (cellulose, hemicellulose, and lignin) [100], the hydrogen bonding interaction can occur between the hydrogen atom (hydroxyl groups) available on the GVWA surface, and the nitrogen (N) atoms in the MB structure (dipole–dipole hydrogen bonding) [101], and between the hydroxyl groups on the GVWA surface and the aromatic rings of MB

Table 6
Linear and non-linear Langmuir parameters and error function for adsorption of dye onto activated grapevine wood

Isotherm model	Parameter values	
	Linear	Non-linear
Langmuir isotherm		
Q_m (mmol·g^{-1})	0.44213	0.689405
K_L (L·mol^{-1})	47.7685	94.9676
R_L	0.9995–0.9985	0.0953–0.0339
R^2	0.9756	0.9869
ARE %	3.9847	2.5966
Freundlich isotherm		
K_F (mmol·g^{-1}(L·mol^{-1})$^{-1/n}$)	3.4709	0.50969
$1/n$	0.8255	0.6933
N	1.2114	1.4424
R^2	0.9638	0.9445
ARE %	2.9795	1.3243
Temkin isotherm		
K_T (L·mol^{-1})	979,540.47	9,085,140.87634
B_T (J·mol^{-1})	1.4953E-5	1.49464E-5
b_T (J·mol^{-1})	168,470,675	168,545,068
R^2	0.9958	0.9968
ARE %	1.1100	1.1071

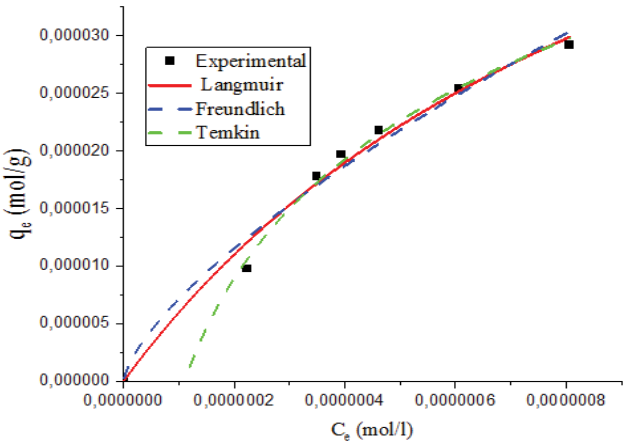

Fig. 17. Comparison of experimental and predicted adsorption isotherms of methylene blue according to Langmuir, Freundlich, and Temkin non-linear models.

Table 7
Maximum adsorption capacity of different adsorbents used for methylene blue dye removal

Adsorbent	Maximum adsorption capacity, Q_m (mg/g)	References
Coconut dregs	5.7208	[81]
Palm kernel shell	16.20	[82]
Seeds of *Citrullus colocynthis* (CCSs)	18.832	[83]
Jack fruit leaf	20.41	[68]
Langsat shell	36.74	[84]
Tea residue	41.84	[85]
Eucalyptus leaves treated with H_3PO_4	50.37	[26]
Cocos nucifera shell treated with H_2SO_4	50.6	[86]
Grape wood wastes activated carbon	62.41	[30]
Jujube shells modified with H_2SO_4	84.5	[24]
Molybdenum trioxide	152	[88]
Didodecyldimethylammonium bromide-modified brown clay (DDAB-BC)	164	[89]
Grapevine wood treated with H_2SO_4	220.51	This study
Wodyetia bifurcata biochar	216.66	[90]
Lotus leaf	241.40	[91]
Banana peel	256.67	[87]
Sugarcane bagasse/HTC with H_3PO_4 + activated with NaOH	357.14	[93]

(Yoshida hydrogen bonding) [102]. The carbonyl groups of the GVWA surface, which serve as electron donors, and the aromatic rings of the MB dye, which serve as electron acceptors, may combine to produce n–π interactions (Fig. 19).

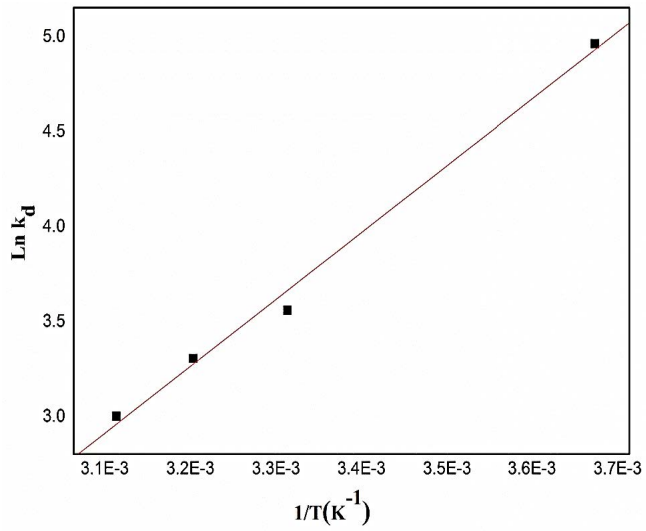

Fig. 18. Shows a van't Hoff plot for methylene blue adsorption on activated grapevine wood.

4. Conclusions

This study showed how to successfully prepare a low-cost biomass adsorbent for the removal of the MB dye using activated grapevine wood biomass GVWA. The best conditions were found by examining the impacts of many parameters, such as particle size, adsorbent dose, agitation speed, pH, temperature, contact time, and initial MB dye concentration. The results showed that increasing the volume and concentration of an aqueous solution of MB, contact time, and temperature resulted in a higher desorption percentage for the H_2SO_4-treated GVW compared with untreated GVW. It had a fast desorption rate of the MB dye and the equilibrium was achieved within 3 h of the equilibration period at 20°C and the normal pH of the MB solution. The results show that non-linear regression was the most effective tool approach to evaluate the kinetic and isotherm variables and select the most acceptable kinetic and isotherm models. The second-order model is suitable for describing the kinetics of MB desorption from dye-loaded adsorbents with a maximum adsorption capacity of MB was 220.51 mg·g^{-1}. This desorption was found to be a spontaneous, endothermic, and progressively random process., according to thermodynamic analyses. This work offered a useful technique for producing a cost-effective, high-performing renewable biosorbent from a variety of biomass. To treat MB in wastewater, the GVWA could be used as a suitable material. This method is successful in removing dyes from

Table 8
Thermodynamic factors of methylene blue dye adsorption onto activated grapevine wood

Temperature (K)	K_d (L·g^{-1})	$\Delta G°$ (kJ·mol^{-1})	$\Delta H°$ (kJ·mol^{-1})	$\Delta S°$ (kJ·mol^{-1}·K^{-1})	R^2
293	135.635	–9.769			
303	33.333	–9.104	–29.325	–0.0665	0.994
313	25.882	–8.439			
323	19.080	–7.774			

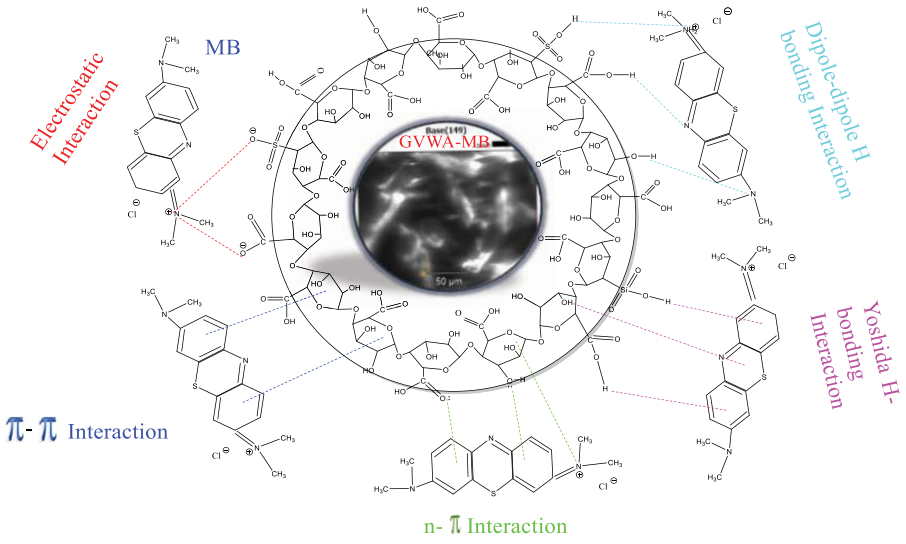

Fig. 19. Possible interactions that may affect how methylene blue adsorbs on activated grapevine wood in an aqueous solution.

aqueous solutions, opening up possibilities for its extension to other types of agricultural waste.

Author contributions

Conceptualization and methodology, R.S., Y.K.; formal analysis, R.S., and S.B.; investigation and data curation S.A., and Y.K., validation L.B.; visualization, original draft preparation, L.B., M.K.A.M, and S.B.; writing—review and editing, S.A., K.B and Y.K.; supervision, L.B., and S.A.

Funding

This research received no external funding.

Informed consent statement

Not applicable.

Data availability statement

Not applicable.

Conflicts of interest

The authors declare no conflict of interest.

References

[1] G.V. Brião, S.L. Jahn, E.L. Foletto, G.L. Dotto, Highly efficient and reusable mesoporous zeolite synthetized from a biopolymer for cationic dyes adsorption, Colloids Surf., A, 556 (2018) 43–50.
[2] D. Georgouvelas, H.N. Abdelhamid, J. Li, U. Edlund, A.P. Mathew, All-cellulose functional membranes for water treatment: adsorption of metal ions and catalytic decolorization of dyes, Carbohydr. Polym., 264 (2021) 118044, doi: 10.1016/J.CARBPOL.2021.118044.
[3] K. Ghosh, N. Bar, A.B. Biswas, S.K. Das, Elimination of crystal violet from synthetic medium by adsorption using unmodified and acid-modified eucalyptus leaves with MPR and GA application, Sustainable Chem. Pharm., 19 (2021) 100370, doi: 10.1016/j.scp.2020.100370.
[4] K.A. Adegoke, O.S. Bello, Dye sequestration using agricultural wastes as adsorbents, Water Resour. Ind., 12 (2015) 8–24.
[5] E. Forgacs, T. Cserhati, G. Oros, Removal of synthetic dyes from wastewaters: a review, Environ. Int., 30 (2004) 953–971.
[6] N. El Messaoudi, M. El Khomri, N. Chlif, Z.G. Chegini, A. Dbik, S. Bentahar, A. Lacherai, Desorption of Congo red from dye-loaded *Phoenix dactylifera* date stones and *Ziziphus lotus* jujube shells, Groundwater Sustainable Dev., 12 (2021) 100552, doi: 10.1016/j.gsd.2021.100552.
[7] S. Darvishmanesh, B.A. Pethica, S. Sundaresan, Forward osmosis using draw solutions manifesting liquid–liquid phase separation, Desalination, 421 (2017) 23–31.
[8] W. Konicki, M. Aleksandrzak, E. Mijowska, Equilibrium, kinetic and thermodynamic studies on adsorption of cationic dyes from aqueous solutions using graphene oxide, Chem. Eng. Res. Des., 123 (2017) 35–49.
[9] V.K. Gupta, Suhas, Application of low-cost adsorbents for dye removal – a review, J. Environ. Manage., 90 (2009) 2313–2342.
[10] N. Wei, X. Zheng, H. Ou, P. Yu, Q. Li, S. Feng, Fabrication of an amine-modified ZIF-8@GO membrane for high-efficiency adsorption of copper ions, New J. Chem., 43 (2019) 5603–5610, doi: 10.1039/C8NJ06521G.
[11] Y. Jia, L. Ding, P. Ren, M. Zhong, J. Ma, X. Fan, Performances and mechanism of methyl orange and Congo red adsorbed on the magnetic ion-exchange resin, J. Chem. Eng. Data, 65 (2020) 725–736.
[12] B. Mu, A. Wang, Adsorption of dyes onto palygorskite and its composites: a review, J. Environ. Chem. Eng., 4 (2016) 1274–1294.
[13] A.S. Abdulhameed, A.H. Jawad, A.-T. Mohammad, Synthesis of chitosan-ethylene glycol diglycidyl ether/TiO_2 nanoparticles for adsorption of Reactive Orange 16 dye using a response surface methodology approach, Bioresour. Technol., 293 (2019) 122071, doi: 10.1016/j.biortech.2019.122071.
[14] M. Sulyman, J. Namiesnik, A. Gierak, Low-cost adsorbents derived from agricultural by-products/wastes for enhancing contaminant uptakes from wastewater: a review, Pol. J. Environ. Stud., 26 (2017) 479–510.
[15] A. Dbik, S. Bentahar, M. El Khomri, N. El Messaoudi, A. Lacherai, Adsorption of Congo red dye from aqueous solutions using tunics of the corm of the saffron, Mater. Today Proc., 22 (2020) 134–139, doi: 10.1016/j.matpr.2019.08.148
[16] M. El Khomri, N. El Messaoudi, A. Dbik, S. Bentahar, Y. Fernine, A. Bouich, A. Lacherai, A. Jada, Modification of low-cost adsorbent prepared from agricultural solid waste for the adsorption and desorption of cationic dye, Emergent Mater., 5 (2022) 1679–1688.
[17] M. El Khomri, N. El Messaoudi, A. Dbik, S. Bentahar, A. Lacherai, N. Faska, A. Jada, Regeneration of argan nutshell and almond shell using HNO_3 for their reusability to remove cationic dye from aqueous solution, Chem. Eng. Commun., 209 (2022) 1304–1315.
[18] M. El Khomri, N. El Messaoudi, A. Dbik, S. Bentahar, Y. Fernine, A. Lacherai, A. Jada, Optimization based on response surface methodology of anionic dye desorption from two agricultural solid wastes, Chem. Afr., 5 (2022) 1083–1095.
[19] M.M. Kwikima, S. Mateso, Y. Chebude, Potentials of agricultural wastes as the ultimate alternative adsorbent for cadmium removal from wastewater. A review, Sci. Afr., 13 (2021) e00934, doi: 10.1016/j.sciaf.2021.e00934.
[20] K. Ghosh, N. Bar, A.B. Biswas, S.K. Das, Elimination of crystal violet from synthetic medium by adsorption using unmodified and acid-modified eucalyptus leaves with MPR and GA application, Sustainable Chem. Pharm., 19 (2021) 100370, doi: 10.1016/j.scp.2020.100370.
[21] I. Ghosh, S. Kar, T. Chatterjee, N. Bar, S.K. Das, Adsorptive removal of Safranin-O dye from aqueous medium using coconut coir and its acid-treated forms: adsorption study, scale-up design, MPR and GA-ANN modeling, Sustainable Chem. Pharm., 19 (2021) 100374, doi: 10.1016/j.scp.2021.100374.
[22] K. Ghosh, N. Bar, G. Roymahapatra, A.B. Biswas, S.K. Das, Adsorptive removal of toxic malachite green from its aqueous solution by *Bambusa vulgaris* leaves and its acid-treated form: DFT, MPR and GA modeling, J. Mol. Liq., 363 (2022) 119841, doi: 10.1016/j.molliq.2022.119841.
[23] V. Russo, D. Masiello, M. Trifuoggi, M. Di Serio, R. Tesser, Design of an adsorption column for methylene blue abatement over silica: from batch to continuous modelling, Chem. Eng. J., 302 (2016) 287–295.
[24] N. El Messaoudi, M. El Khomri, Z. Goodarzvand Chegini, N. Chlif, A. Dbik, S. Bentahar, M. Iqbal, A. Jada, A. Lacherai, Desorption study and reusability of raw and H_2SO_4 modified jujube shells (*Zizyphus lotus*) for the methylene blue adsorption, Int. J. Environ. Anal. Chem., (2021), doi: 10.1080/03067319.2021.1912338.
[25] I. Ghosh, S. Kar, T. Chatterjee, N. Bar, S.K. Das, Removal of methylene blue from aqueous solution using *Lathyrus sativus* husk: adsorption study, MPR and ANN modeling, Process Saf. Environ. Prot., 149 (2021) 345–361.
[26] K. Ghosh, N. Bar, A.B. Biswas, S.K. Das, Removal of methylene blue by H_3PO_4-treated eucalyptus leaves: study of fixed bed column and GA-ANN modeling, Sustainable Chem. Pharm., 29 (2022) 100774, doi: 10.1016/j.scp.2022.100774.
[27] D.M.N.H. Jayasuriya, K. Nadarajah, Understanding association between methylene blue dye and biosorbent: Palmyrah sprout casing in adsorption process in aqueous phase, Water Sci. Eng., (2023), doi: 10.1016/j.wse.2022.12.006.
[28] X. Sun, X. Wei, J. Zhang, Q. Ge, Y. Liang, Y. Ju, A. Zhang, T. Ma, Y. Fang, Biomass estimation and physicochemical

characterization of winter vine prunings in the Chinese and global grape and wine industries, Waste Manage., 104 (2020) 119–129.
[29] S.O. Prozil, E.V. Costa, D.V. Evtuguin, L.P.C. Lopes, M.R.M. Domingues, Structural characterization of polysaccharides isolated from grape stalks of *Vitis vinifera* L., Carbohydr. Res., 356 (2012) 252–259.
[30] S.A. Mousavi, D. Shahbazi, A. Mahmoudi, P. Darvishi, Methylene blue removal using prepared activated carbon from grape wood wastes: adsorption process analysis and modelling, Water Qual. Res. J., 57 (2022) 1–19.
[31] L. Giraldo-Gutiérrez, J.C. Moreno-Piraján, Pb^{2+} adsorption from aqueous solutions on activated carbons obtained from lignocellulosic residues, Braz. J. Chem. Eng., 25 (2008) 143–151.
[32] F. Rodriguez-Reinoso, The role of carbon materials in heterogeneous catalysis, Carbon, 36 (1998) 159–175.
[33] G. Crini, P.M. Badot, Traitement et épuration des eaux industrielles polluées, Presses Universitaires de Franche Comté, Besançon, France, 2007.
[34] V.H. Vargas, R.R. Paveglio, P. de S. Pauletto, N.P.G. Salau, L.G. Dotto, Sisal fiber as an alternative and cost-effective adsorbent for the removal of methylene blue and Reactive Black 5 dyes from aqueous solutions, Chem. Eng. Commun., 207 (2020) 523–536.
[35] J. Guo, A.C. Lu, Transaction IChemE: Chemical Engineering Research & Design. 81, Part A, UK, 2003, pp. 585–590.
[36] M. Bounaas, A. Bouguettoucha, D. Chebli, J.M. Gatica, H. Vidal, Role of the wild carob as biosorbent and as precursor of a new high-surface-area activated carbon for the adsorption of methylene blue, Arabian J. Sci. Eng., 46 (2021) 325–341.
[37] S. Zhu, J. Xu, Y. Kuang, Z. Cheng, Q. Wu, J. Xie, B. Wang, W. Gao, J. Zeng, J. Li, K. Chen, Lignin-derived sulfonated porous carbon from cornstalk for efficient and selective removal of cationic dyes, Ind. Crops Prod., 159 (2021) 113071, doi: 10.1016/j.indcrop.2020.113071.
[38] S. Bhattacharya, N. Bar, B. Rajbansi, S.K. Das, Adsorptive elimination of Cu(II) from aqueous solution by chitosan-nanoSiO_2 nanocomposite—adsorption study, MLR, and GA modeling, Water Air Soil Pollut., 232 (2021) 161, doi: 10.1007/s11270-021-05070-x.
[39] S. Benyoucef, Dj. Harrache, Caractérisation de la microstructure de sciure de bois de pin sylvestre "*Pinus sylvestris*" (Microstructure characterization of scots pine "*Pinus sylvestris*" sawdust), J. Mater. Environ. Sci., 6 (2015) 765–772.
[40] L. Segal, J.J. Creely, A.E. Martin, C.M. Conrad, An empirical method for estimating the degree of crystallinity of native cellulose using the X-ray diffractometer, Text. Res. J., 29 (1959) 786–794.
[41] M.F. Rosa, E.S. Medeiros, J.A. Malmonge, K.S. Grégorski, D.F. Wood, L.H.C. Mattoso, G. Glenn, W.J. Orts, S.H. Imam, Cellulose nanowhiskers from coconut husk fibers: effect of preparation conditions on their thermal and morphological behavior, Carbohydr. Polym., 81 (2010) 83–92.
[42] D. Klemm, B. Heublein, H.P. Fink, A. Bohn, Cellulose: fascinating biopolymer and sustainable raw material, Angew. Chem. Int. Ed., 44 (2005) 3358–3393.
[43] A. Alemdar, M. Sain, Isolation and characterization of nanofibers from agricultural residues – wheat straw and soy hulls, Bioresour. Technol., 99 (2008) 1664–1671.
[44] I. Shahabi-Ghahafarrokhi, F. Khodaiyan, M. Mousavi, H. Yousefi, Preparation and characterization of nanocellulose from beer industrial residues using acid hydrolysis/ultrasound, Fibers Polym., 16 (2015) 529–536.
[45] S. Brunauer, P.H. Emmett, E. Teller, Adsorption of gases in multimolecular layers, J. Am. Chem. Soc., 60 (1938) 309–319.
[46] I. Ghosh, S. Kar, T. Chatterjee, N. Bar, S.K. Das, Removal of methylene blue from aqueous solution using *Lathyrus sativus* husk: adsorption study, MPR and ANN modelling, Process Saf. Environ. Prot., 149 (2021) 345–361.
[47] J.J. Salazar-Rabago, R. Leyva-Ramos, J. Rivera-Utrilla, R. Ocampo-Perez, F.J. Cerino-Cordova, Biosorption mechanism of methylene blue from aqueous solution onto White Pine (*Pinus durangensis*) sawdust: effect of operating condition, Sustainable Environ. Res., 27 (2017) 32–40.
[48] J.F. Fiset, J.F. Blais, R. Ben cheick, R. Dayal Tyagi, Revue sur l'enlèvement des métaux des effluents par adsorption sur la sciure et les écorces de bois, Revue des sciences de l'eau, 13 (2001) 323–347.
[49] M. Ali Rehab, A. Hamad Hesham, M.M. Hussein, G.F. Malash, Potential of using green adsorbent of heavy metal removal from aqueous solutions: adsorption kinetics, isotherm, thermodynamic, mechanism and economic analysis, Ecol. Eng., 91 (2016) 317–332.
[50] M.A. Al-Ghouti, R.S. Al-Absi, Mechanistic understanding of the adsorption and thermodynamic aspects of cationic methylene blue dye onto cellulosic olive stones biomass from wastewater, Sci. Rep., 10 (2020) 15928, doi: 10.1038/s41598-020-72996-3.
[51] L. Seo-Yun, C. Hee-Jeong, Efficient adsorption of methylene blue from aqueous solution by sulfuric acid activated watermelon rind (*Citrullus lanatus*), Appl. Chem. Eng., 32 (2021) 348–356.
[52] H. Aysan, S. Edebali, C. Ozdemir, M.C. Karakaya, N. Karakaya, Use of chabazite, a naturally abundant zeolite, for the investigation of the adsorption kinetics and mechanism of methylene blue dye, Microporous Mesoporous Mater., 235 (2016) 78–86.
[53] K. Enenebeaku Conrad, J. Okorocha Nnaemeka, E. Enenebeaku Uchechi, I. Onyeachu Benedict, Adsorption of methylene blue dye onto bush cane bark powder international letters of chemistry, Phys. Astron., 32 (2021) 348–356.
[54] F. Marrakchi, W.A. Khanday, M. Asif, B.H. Hameed, Cross-linked chitosan/sepiolite composite for the adsorption of methylene blue and Reactive Orange 16, Int. J. Biol. Macromol., 93 (2016) 1231–1239.
[55] Q.-X. Liu, Y.-R. Zhou, M. Wang, Q. Zhang, T. Ji, T.-Y. Chen, D.-C. Yu, Adsorption of methylene blue from aqueous solution onto viscose-based activated carbon fiber felts: kinetics and equilibrium studies, Adsorpt. Sci. Technol., 37 (2019) 312–332.
[56] A.H. Jawad, R.A. Rashid, M.A.M. Ishak, L.D. Wilson, Adsorption of methylene blue onto activated carbon developed from biomass waste by H_2SO_4 activation: kinetic, equilibrium and thermodynamic studies, Desal. Water Treat., 57 (2016) 25194–25206.
[57] A.H. Jawad, N.F. Hanani Mamat, M.F. Abdullah, K. Ismail, Adsorption of methylene blue onto acid-treated mango peels: kinetic, equilibrium and thermodynamic study, Desal. Water Treat., 59 (2017) 210–219.
[58] N. El Messaoudi, M. El Khomri, Y. Fernine, A. Bouich, A. Lacherai, A. Jada, F. Sher, E.C. Lima, Hydrothermally engineered *Eriobotrya japonica* leaves/MgO nanocomposites with potential applications in wastewater treatment, Groundwater Sustainable Dev., 16 (2022) 100728, doi: 10.1016/j.gsd.2022.100728.
[59] M.K. Uddin, A. Nasar, Walnut shell powder as a low-cost adsorbent for methylene blue dye: isotherm, kinetics, thermodynamic, desorption and response surface methodology examinations, Sci. Rep., 10 (2020) 7983, doi: 10.1038/s41598-020-64745-3.
[60] N. El Messaoudi, M. El Khomri, E.-H. Ablouh, A. Bouich, A. Lacherai, A. Jada, E.C. Lima, F. Sher, Biosynthesis of SiO_2 nanoparticles using extract of *Nerium oleander* leaves for the removal of tetracycline antibiotic, Chemosphere, 287 (2022) 132453, doi: 10.1016/j.chemosphere.2021.132453.
[61] R. Tang, C. Dai, C. Li, W. Liu, S. Gao, C. Wang, Removal of methylene blue from aqueous solution using agricultural residue walnut shell: equilibrium, kinetic, and thermodynamic studies, J. Chem., 2017 (2017) 1–10, doi: 10.1155/2017/8404965.
[62] A. Aichour, H. Zaghouane-Boudiaf, C.V. Iborra, M.S. Polo, Bioadsorbent beads prepared from activated biomass/alginate for enhanced removal of cationic dye from water medium: kinetics, equilibrium and thermodynamic studies, J. Mol. Liq., 256 (2018) 533–540.
[63] M. Khodaie, N. Ghasemi, B. Moradi, M. Rahimi, Removal of methylene blue from wastewater by adsorption onto $ZnCl_2$

activated corn husk carbon equilibrium studies, J. Chem., 2013 (2013) 1–6, doi: 10.1155/2013/383985.
[64] Md. Zahanggir Alam, Md. Niamul Bari, K. Sayera, Statistical optimization of methylene blue dye removal from a synthetic textile wastewater using indigenous adsorbents, Environ. Sustainability Indic., 14 (2022) 100176, doi: 10.1016/j.indic.2022.100176.
[65] S. Lagergren, Zur theoric der sogenannten adsorption geloster stoffe (About the theory of so-called adsorption of soluble substances), Kungliga SvenskaVetenskapsakademiens. Handlingar, 24 (1898) 1–39.
[66] Y.S. Ho, G. McKay, The kinetics of sorption of divalent metal ions onto sphagnum moss peat, Water Res., 34 (2000) 735–742.
[67] W.J. Weber, J.C. Morris, Kinetics of adsorption on carbon from solution, J. Sanit. Eng. Div., Proc. Am. Soc. Civ. Eng., 89 (1963) 31–59.
[68] S. Banerjee, A. Debsarkar, S. Datta, Adsorption of methylene blue and malachite green in aqueous solution using jack fruit leaf ash as low cost adsorbent, Int. J. Environ. Agric. Biotechnol. (IJEAB), 2 (2017) 2456–1878.
[69] S. Yanasinee, P. Nittaya, E. Numfon, Adsorption of methylene blue by low-cost biochar derived from elephant dung. Appl. Environ. Res., 43 (2021) 34–44.
[70] S. Zhu, J. Xu, Y. Kuang, Z. Cheng, Q. Wu, J. Xie, B. Wang, W. Gao, J. Zeng, J. Li, K. Chen, Lignin-derived sulfonated porous carbon from cornstalk for efficient and selective removal of cationic dyes, Ind. Crops Prod., 159 (2021) 113071, doi: 10.1016/j.indcrop.2020.113071.
[71] N. Hasani, T. Selimi, A. Mele, V. Thaçi, J. Halili, A. Berisha, M. Sadiku, Theoretical, equilibrium, kinetics and thermodynamic investigations of methylene blue adsorption onto lignite coal, Molecules, 27 (2022) 1856, doi: 10.3390/molecules 27061856.
[72] I. Nouacer, M. Benalia, G. Henini, M. Djedid, Y. Laidani, Mathematical modeling and interpretation of equilibrium isotherms of Pb(II) from aqueous media by *Chlorella pyrenoidosa* immobilized in *Luffa cylindrica*, Biomass Convers. Biorefin., (2021), doi: 10.1007/s13399-021-01722-4.
[73] I. Langmuir, The adsorption of gases on plane surfaces of glass, mica and platinum, J. Am. Chem. Soc., 40 (1918) 1361–1403.
[74] K R. Hall, L.C. Eagleton, A. Acrivos, T. Vermeulen, Pore- and solid-diffusion kinetics in fixed-bed adsorption under constant-pattern conditions, Ind. Eng. Chem. Fundam., 5 (1966) 212–223.
[75] H.M.F. Freundlich, Over the adsorption in solution, Ind. Eng. Chem., 57 (1906) 385–470.
[76] M.A. Rauf, S.B. Bukallah, FA. Hamour, A.S. Nasir, Adsorption of dyes from aqueous solutions onto sand and their kinetic behavior, Chem. Eng. J., 137 (2008) 238–243.
[77] A. Savran, N.Ç. Selçuk, Ş. Kubilay, A.R. Kul, Adsorption isotherm models for dye removal by *Paliurus spinachristi* mill. frutis and seeds in a single component system, IOSR J. Environ. Sci. Toxicol. Food Technol., 11 (2017) 18–30.
[78] M.J. Temkin, V. Pyzhev, Recent modifications to Langmuir isotherms, Acta Physiochim. URSS, 12 (1940) 217–222.
[79] T. Ahmed, W. Noor, O. Faruk, M.C. Bhoumick, M.T. Uddin, Removal of methylene blue (MB) from wastewater by adsorption on jackfruit leaf powder (JLP) in continuously stirred tank reactor, J. Phys. Conf. Ser., 1086 (2018) 012012, doi: 10.1088/1742-6596/1086/1/012012.
[80] K. Ghosh, N. Bar, A.B. Biswas, S.K. Das, Removal of methylene blue by H_3PO_4-treated eucalyptus leaves: study of fixed bed column and GA-ANN modeling, Sustainable Chem. Pharm., 29 (2022) 100774, doi: 10.1016/j.scp.2022.100774.
[81] H. Shukor, A.Z. Yaser, N.F. Shoparwe, M.M.Z. Makhtar, N. Mokhtar, Biosorption study of methylene blue (MB) and Brilliant Red Remazol (BRR) by coconut dregs, Int. J. Chem. Eng., 2022 (2022) 8153617, doi: 10.1155/2022/8153617.
[82] N. Benjamen, A.O. Salaudeen, J.U. Utam, Isotherm studies of adsorption of methylene blue by palm kernel shell, Asian J. Appl. Chem. Res., 1 (2018) 1–9.
[83] W.M. Alghamdi, I. El Mannoubi, Investigation of seeds and peels of *Citrullus colocynthis* as efficient natural adsorbent for methylene blue dye, Processes, 9 (2021) 1279, doi: 10.3390/pr9081279.
[84] D. Kurniawati, S. Bahrizal, T.K. Sari, F. Adella, Sy. Salmariza, Effect of contact time adsorption of Rhodamine B, Methyl Orange and methylene blue colours on Langsat shell with batch methods, J. Phys. Conf. Ser., 1788 (2021) 012008, doi: 10.1088/1742-6596/1788/1/012008.
[85] T.T.C. Truong, N.T.T. Vo, K.D. Nguyen, H.M. Bui, Preparation of cellulose-based hydrogel derived from tea residue for the adsorption of methylene blue, Cellul. Chem. Technol., 53 (2019) 573–582.
[86] A.H. Jawad, A.S. Abdulhameed, M. Sufri Mastuli, Acid-factionalized biomass material for methylene blue dye removal: a comprehensive adsorption and mechanism study, J. Taibah Univ. Sci., 14 (2020) 305–313.
[87] S.A. Mousavi, D. Shahbazi, A. Mahmoudi, P. Darvishi, Methylene blue removal using prepared activated carbon from grape wood wastes: adsorption process analysis and modelling, Water Qual. Res. J., 57 (2021) 1–19, doi: 10.2166/wqrj.2021.015.
[88] S. Rakass, H. Oudghiri Hassani, M. Abboudi, F. Kooli, A. Mohmoud, A. Aljuhani, F. Al Wadaani, Molybdenum trioxide: efficient nanosorbent for removal of methylene blue dye from aqueous solutions, Molecules, 23 (2018) 2295, doi: 10.3390/molecules23092295.
[89] M. Munir, M.F. Nazar, M.N. Zafar, M. Zubair, M. Ashfaq, A. Hosseini-Bandegharaei, S. Ud-Din Khan, A. Ahmad, Effective adsorptive removal of methylene blue from water by didodecyldimethylammonium bromide-modified brown clay, ACS Omega, 5 (2020) 16711–16721.
[90] K.J.L. dos Santos, G.E. de Souza dos Santos, I.M.G. de Sá, A.H. Ide, J.L. da Silva Duarte, S.H. Vieira de Carvalho, J.I. Soletti, L. Meili, *Wodyetia bifurcata* biochar for methylene blue removal from aqueous matrix, Bioresour. Technol., 293 (2019) 122093, doi: 10.1016/j.biortech.2019.122093.
[91] H. Xiuli, W. Wei, M. Xiaojian, Adsorption characteristics of methylene blue onto low-cost biomass material lotus leaf, Int. J. Eng. Technol., 7 (2018) 3007–3013.
[92] H. Kayaalp, S. Savcı, R. Coşkun, Y. Mutlu, Adsorption of methylene blue from aqueous solution with vermicompost produced using banana peel, Int. J. Mod. Eng. Res. (IJMER), 7 (2017) 64–73.
[93] F. Zhou, K. Li, F. Hang, Z. Zhang, P. Chen, L. Wei, C. Xie, Efficient removal of methylene blue by activated hydrochar prepared by hydrothermal carbonization and NaOH activation of sugarcane bagasse and phosphoric acid, RSC Adv., 12 (2022) 1885, doi: 10.1039/D1RA08325B.
[94] N.Y. Mezenner, A. Bensmaili, Kinetics and thermodynamic study of phosphate adsorption on iron hydroxide-eggshell waste, Chem. Eng. J., 147 (2009) 87–96.
[95] A. Das, N. Bar, S.K. Das, Adsorptive removal of Pb(II) ion on *Arachis hypogaea*'s shell: batch experiments, statistical, and GA modeling, Int. J. Environ. Sci. Technol., 20 (2023) 537–550.
[96] P. Suresh Kumar, L. Korving, M.C.M. van Loosdrecht, G.-J. Witkamp, Adsorption as a technology to achieve ultra-low concentrations of phosphate: research gaps and economic analysis, Water Res. X, 4 (2019) 100029, doi: 10.1016/j.wroa.2019.100029.
[97] A.M. Awwad, N.M. Salem, Kinetics and thermodynamics of Cd(II) biosorption onto loquat (*Eriobotrya japonica*) leaves, J. Saudi Chem. Soc., 18 (2014) 486–493.
[98] H.J. Choi, S.W. Yu, Biosorption of methylene blue from aqueous solution by agricultural bioadsorbent corncob, Environ. Eng. Res., 24 (2019) 99–106.
[99] A. Dbik, S. Bentahar, N. El Messaoudi, M. El Khomri, A. Lacherai, Removal of methylene blue from aqueous solution by tunics of the corm of the saffron, Iran. J. Chem. Chem. Eng., 39 (2020).

[100] E. Santoso, R. Ediati, Y. Kusumawati, H. Bahruji, D.O. Sulistiono, D. Prasetyoko, Review on recent advances of carbon based adsorbent for methylene blue removal from wastewater, Mater. Today Chem., 16 (2020) 100233, doi: 10.1016/j.mtchem.2019.100233.
[101] R.W. Sabnis, Handbook of Biological Dyes and Stains: Synthesis and Industrial Applications, A John Wiley & Sons, Inc., Hoboken, New Jersey, 2010.
[102] H.N. Tran, S.-J. You, T.V. Nguyen, H.-P. Chao, Insight into the adsorption mechanism of cationic dye onto biosorbents derived from agricultural wastes, Chem. Eng. Commun., 204 (2017) 1020–1036.